

# An EFT origin of Secluded Dark Matter

---

**Asesh Krishna Datta,<sup>a</sup> Sourov Roy,<sup>b</sup> Abhijit Kumar Saha<sup>c</sup> Ananya Tapadar<sup>b</sup>**

<sup>a</sup>*Harish-Chandra Research Institute, A CI of Homi Bhabha National Institute (HBNI),  
Chhatnag Road, Jhusi, Prayagraj (Allahabad), Uttar Pradesh 211019, India*

<sup>b</sup>*School of Physical Sciences, Indian Association for the Cultivation of Science,  
2A & 2B Raja S.C. Mullick Road, Jadavpur, Kolkata 700 032, India*

<sup>c</sup>*Institute of Physics, Sachivalaya Marg, Bhubaneswar 751005, Orissa, India*

*E-mail:* [asesh@hri.res.in](mailto:asesh@hri.res.in), [tpsr@iacs.res.in](mailto:tpsr@iacs.res.in), [abhijit.saha@iopb.res.in](mailto:abhijit.saha@iopb.res.in),  
[intat@iacs.res.in](mailto:intat@iacs.res.in)

**ABSTRACT:** The present study aims to unveil a non-minimal secluded dark sector (DS) scenario in an effective field theory (EFT) framework. To explore this, we have examined a suitable extension of type-X Two Higgs Doublet Model (2HDM) as a potential origin for secluded DS. The dark sector, possessing non-minimal characteristics, becomes non-thermally populated through diverse dim-6 four-Fermi operators, effectively generated by integrating out the heavier Higgs particles. The analysis further focuses on the consequence of the collision mechanism  $DM + a \rightarrow a + a$ , occurring within the DS, where ‘ $a$ ’ represents the lighter DS particle. We have investigated the significance of employing an effective theory approach to track the temperature evolution of the dark sector (DS). Within the present framework, the final relic abundance of dark matter can be attained through both dark freeze-out and freeze-in mechanisms. Furthermore, we have delineated the permissible ranges of relevant parameter space essential for achieving the correct dark matter relic abundance considering different variants of cosmology, as validated by Big Bang Nucleosynthesis (BBN) and gamma-ray searches.

---

## Contents

<b>1</b>	<b>Introduction</b>	<b>1</b>
<b>2</b>	<b>The Model</b>	<b>3</b>
<b>3</b>	<b>A brief note on non-standard cosmology</b>	<b>5</b>
<b>4</b>	<b>Studying the Boltzmann equations</b>	<b>6</b>
4.1	Formulation of the Boltzmann equations	7
4.2	An analytic understanding of the Boltzmann equations	8
<b>5</b>	<b>Results</b>	<b>10</b>
5.1	The region (out) of thermal equilibrium	11
5.2	Numerical study of Boltzmann equations	12
5.3	Constraints from the Big Bang Nucleosynthesis	15
5.4	Indirect detection of the DM in gamma ray searches	17
<b>6</b>	<b>Summary and Conclusions</b>	<b>19</b>
<b>7</b>	<b>Acknowledgement</b>	<b>21</b>

---

## 1 Introduction

The existence of dark matter (DM) has now been firmly established through various astrophysical and cosmological observations [1–5]. However, the particle nature of DM and its interactions with the Standard Model (SM) fields are still unknown. Given that there is no viable candidate for the DM in the spectrum of the SM, this has led several decades into intense exploration of potential physics scenarios beyond the SM (BSM) possessing a DM particle of varying nature and prompted us to take up detailed studies of plausible cosmological mechanisms that could generate the experimentally observed relic abundance of DM.

Amidst these discussions, one of the prominently debated topics aiming to elucidate the particle nature of dark matter is the concept of Weakly Interacting Massive Particles (WIMPs) [6–9]. In the WIMP paradigm, the DM is expected to be in thermal equilibrium at early Universe and would decouple from the thermal bath at a later stage leading to their freeze-out. The fact that masses and couplings at the weak scale lead to a WIMP abundance that matches the observed dark matter energy density is commonly known as the “WIMP miracle” [10]. Nevertheless, despite their appeal, WIMPs have evaded detection so far. The absence of any convincing signature of the DM in the direct and indirect searches severely restricts viability of a WIMP DM [11–15]. The null results at these DM search experiments might as well hint at the possibility of new production mechanisms of DM in thermal and non-thermal scenarios.

A new freeze-out mechanism for the thermal DM freeze-out has been proposed in [16, 17], where the dark matter relic abundance is determined solely by the co-annihilation of DM with one or more lighter species, via DM  $a \rightarrow aa$  process, where ‘ $a$ ’ is any lighter mass particle present in the thermal bath. If the final relic abundance of DM has its origin in such co-scattering [16, 18–20] processes, then its coupling could be exponentially smaller to reproduce correct relic abundance, compared to the coupling required for the WIMP scenario. This particular nature is prompted in the chemical phase, when, larger abundance of lighter species increases the reaction rate, resulting into a smaller coupling. Hence this process facilitates having a significantly heavier DM with an interaction strength very similar to what is required for WIMP freeze-out.

However, it is possible that, in the early Universe, the DM has very feeble interactions to particles in the thermal bath and hence never reaches thermal equilibrium. Under such circumstances, the so called freeze-in mechanism [21–23] could still give rise to the observed DM relic abundance. Alternatively, it is also possible that a particle DM is an SM singlet and it resides inside a dark sector (DS) which remains thermally decoupled (secluded) from the visible sector (VS). However, a strong conversion process inside the DS allows the DM to reach internal thermal equilibrium [24–32]. In this case, the evolutions of the DS temperature ( $T_D$ ) and the VS temperature ( $T$ ) turn out to be significantly different [24, 25, 28–30, 33]. In fact, the ratio  $\frac{T_D}{T}$  crucially depends on how the DS particles were originally produced and the cosmology that governs the early Universe. In case of a minimal secluded DS scenario, the DM depletes through annihilation to itself via DM number changing self interaction processes [32, 34]. However, in a scenario with a non-minimal secluded sector, DM annihilates into lighter DS states via DM DM  $\rightarrow aa$  scattering process where ‘ $a$ ’ (mediator particle) is the lighter DS particle, where ‘ $a$ ’ may possess feeble couplings to the VS particles [25, 35, 36].

In this work, we plan to investigate a generic scenario where DM  $a \rightarrow aa$  scattering process takes place in a thermally decoupled or a secluded dark sector along with how the DS gets populated in the first place. Here, we have assumed that the DS comprises of a single dark matter candidate ( $\chi$ ) and a mediator particle ( $\xi$ ) (can be identified with ‘ $a$ ’ above), which are fermionic in nature. The population of the DS is aided by the VS through a series of dim-6 four-Fermi vertex operators. These operators are formulated within the framework of an effective field theory (EFT) derived from a UV-complete model. The UV complete model studied in this context is an extended version of Type-X two Higgs Doublet Model (2HDM). In order to introduce Yukawa like portal interactions between the DS and the VS, we introduce 2HDM and the requirements of only lepton specific portal couplings lead us to the choice of Type-X. Such an extended Type-X 2HDM with lepton specific portal interactions is motivated by different astrophysical and cosmological observations. Here, we have introduced a global  $U(1)_{e-\mu}$  symmetry which incorporates the portal couplings between  $\xi$  and  $e, \mu$  flavoured leptons. However, one may also choose a global  $U(1)_{e-\tau}$  symmetry for the portal couplings.

Further, we have assumed the BSM Higgs states to be heavy enough and hence can be integrated out below the effective scale ( $\Lambda$ ). This results into the relevant operators that trigger populating the DS in the first place. To study the phases of the dark sector, we also calculate the dark sector temperature  $T_D$  by considering all the possible production channels of  $\xi$  followed by an instantaneous production of  $\chi$  from  $\xi$ . As the Universe cools down ( $T_D < m_\chi$ ),  $\chi$  annihilates into  $\xi$  via the processes  $\bar{\xi}\chi \rightarrow \bar{\xi}^c\xi$  and  $\bar{\chi}\chi \rightarrow \bar{\xi}\xi$  thus leading to its freeze-out. Additionally, the correct

relic abundance of  $\chi$  can also be generated through the freeze-in mechanism with a small coupling strength within the DS. The stability of  $\chi$  is ensured by considering  $m_\xi < m_\chi < 3m_\xi$  along with the smallness of the portal coupling between the DS and the VS. Here, we have solved three Boltzmann equations simultaneously, which govern the number density of  $\xi$  and  $\chi$  and the total energy density ( $\rho_D$ ) of DS.

Furthermore, the smallness of the portal coupling allows for decays of  $\xi$  into SM leptons, in particular, into neutrinos and electrons, at a later stage, which might jeopardize the successful predictions of the Big Bang Nucleosynthesis (BBN). To avoid this, we have constrained the relevant portal coupling so that  $\xi$  decays before BBN. Additionally, the coupling strength involved in DM self-annihilation into a pair of mediator particles (which could decay to charged leptons that radiate photons) can also be probed by gamma-ray observatories such as Fermi-LAT [37–39].

The paper is structured as follows. In section 2 we briefly describe the model under consideration and write down the relevant effective operators. Section 3 presents a discussion on non-standard cosmology that we have explored in this work. Section 4 and 5 are devoted to a detailed analysis of Boltzmann equations and the corresponding numerical results including studies on the constraints on the model from the BBN and the prospects for indirect detection of DM from gamma-ray searches. Our summary and conclusions are presented in section 6.

## 2 The Model

In this study, we have investigated the type-X 2HDM model [40, 41] by augmenting it with a DS comprises of a SM gauge singlet scalar ( $S$ ) and two Dirac Fermions: one acting as the mediator particle ( $\xi$ ) while the other ( $\chi$ ) proposed as the candidate for dark matter. We have introduced a global  $U(1)_{e-\mu}$  symmetry, assigning nontrivial charges to  $S$ ,  $\xi$ , and  $\chi$ , as detailed in table 1. The interactions that are relevant for this work are all contained in the Yukawa sector of the Lagrangian which are given as follows:

$$\mathcal{L} \supset y_{1i} \bar{L}_i \Phi_1 e_{R_i} + y_{2i} \bar{Q}_i \Phi_2 d_{R_i} + y_{3i} \bar{Q}_i \Phi_2^c u_{R_i} + y_4 \bar{L}_e \Phi_1^c \xi_R + y_5 \bar{L}_\mu \Phi_1^c \xi^c_R + y_6 S \bar{\xi}^c \xi + y_7 S \bar{\xi} \chi + h.c., \quad (2.1)$$

where,  $\Phi_1$  and  $\Phi_2$  represent two distinct  $SU(2)_L$  Higgs doublets. Notably,  $\Phi_1$  exclusively couples to SM leptons, while  $\Phi_2$  interacts exclusively with SM quarks. This coupling arrangement is specific to type-X 2HDM and usually achieved by enforcing a  $Z_2$  symmetry [42], wherein  $\Phi_2$ , along with the right-handed up-type quarks  $u_{R_i}$  and right-handed down-type quarks  $d_{R_i}$ , exhibit odd parity under this symmetry. On the electroweak symmetry breaking, the scenario gives rise to three Goldstone bosons that contribute to the longitudinal modes of the massive  $W^\pm$  and  $Z$  bosons. Additionally, the spectrum contains five massive scalar degrees of freedom: two CP-even states ( $h, H$ ), one CP-odd state ( $A$ ), and a pair of charged Higgs states ( $H^\pm$ ). Here, both  $\Phi_1$  and  $\Phi_2$  acquire non-zero VEVs  $v_1$  and  $v_2$ , respectively, with,  $v_{\text{SM}} = \sqrt{v_1^2 + v_2^2} = 246 \text{ GeV}$ . The scalar doublets  $\Phi_1$  and  $\Phi_2$ , in terms of the physical scalar states, can be written as,

$$\Phi_1 = \begin{pmatrix} -H^+ \sin \beta \\ \sqrt{\frac{1}{2}}(v_1 + H \cos \alpha - h \sin \alpha - i A \sin \beta) \end{pmatrix}, \quad (2.2)$$

$$\Phi_2 = \begin{pmatrix} H^+ \cos \beta \\ \sqrt{\frac{1}{2}}(v_2 + H \sin \alpha + h \cos \alpha + i A \cos \beta) \end{pmatrix}, \quad (2.3)$$

Fields	$U(1)_{e-\mu}$
$\xi$	1
$S$	-2
$\chi$	3

**Table 1.**  $U(1)_{L_e-L_\mu}$  charge assignments for the BSM gauge singlet fields.

where,  $\tan \beta = \frac{v_2}{v_1}$  and ‘ $\alpha$ ’ parameterized the mixing between the gauge and mass eigenstates of the CP-even Higgs bosons. In the alignment limit i.e.  $\beta - \alpha = \frac{\pi}{2}$ , ‘ $h$ ’ can be identified with the observed SM like Higgs boson having a mass  $\simeq 125$  GeV [40, 43].

The Yukawa couplings  $y_{1i}$ ,  $y_{2i}$  and  $y_{3i}$  are given by,

$$y_{1i} = \frac{g m_{e_i}}{\sqrt{2} m_W \cos \beta}, \quad y_{2i} = \frac{g m_{u_i}}{\sqrt{2} m_W \sin \beta}, \quad y_{3i} = \frac{g m_{d_i}}{\sqrt{2} m_W \sin \beta}, \quad (2.4)$$

where  $e_i = \{e, \mu, \tau\}$ ,  $u_i = \{u, c, t\}$  and  $d_i = \{d, s, b\}$ , include different generations of leptons, up-type and down type quarks, respectively and  $m_{e_i}$ ,  $m_{u_i}$  and  $m_{d_i}$  are the corresponding masses. The mass of the  $W$  gauge boson is given by  $m_W$ , while ‘ $g$ ’ represents the  $SU(2)_L$  gauge coupling. It may be noted that the most conservative upper limit on  $\tan \beta$  comes from considering  $y_{1\tau} < 4\pi$  and is given by,

$$\tan \beta \lesssim 1255. \quad (2.5)$$

As for the interactions involving the DS particles, the existence of a global  $U(1)_{e-\mu}$  symmetry dictates that only the fourth and fifth terms in the Eq. (2.1) are permissible as portal couplings linking the DS and the VS. Also for the same reason last two terms in Eq. (2.1) are the only allowed ones that govern the interactions of DS particles among themselves. In subsequent sections, we will delve into the impact of these terms on the production mechanisms of the DS particles, the relic abundance of DM and its detection prospects.

We impose a mass hierarchies of  $m_{S,H,A,H^\pm} \gg m_{\chi,\xi}$ , which enables us to adopt an effective field theory framework with an effective scale  $\Lambda$ . The coupling of  $\xi$  with the SM Higgs boson ( $h$ ) is suppressed by  $\tan \beta$  and can be safely ignored for our purpose. To ensure a reasonably accurate approach to EFT at high temperature i.e. DS particles are relativistic to start with, we set  $\Lambda = 100 m_\chi$ . Consequently, below this cut-off scale, on integrating out the heavier Higgs fields, several dim-6 six four-Fermi operators emerge that contribute significantly to the production of the DS particles in the early Universe. The specific dim-6 operators are listed in table 2. The Yukawa couplings  $y_{1i}$  are fixed by the masses of the leptons for a given  $\tan \beta$ , whereas  $y_4$ ,  $y_5$  are the free parameter of the theory. Here,  $y_{2i}$ ,  $y_{3i}$  are also fixed by SM quark masses, ‘ $i$ ’ being quark the generation index. Note that,  $y_{2i}$ ,  $y_{3i}$  do not contribute to the DS phenomenology since the quarks do not interact with the DS particles. It is further important to note that, the requirement of non-thermal production of DS forces  $y_4$  and  $y_5$  to be very small as compared to  $y_{1i}, y_{2i}$  and which in terms make  $C_3$ ,  $C_4$  and  $C_5$  significantly suppressed. We also note due to the known mass (Yukawa coupling) hierarchies of the SM leptons, the primary contribution to the non-thermal production of the DS particles will predominantly come from terms involving the coefficient of  $C_{1\tau}$ ,  $C_{2\tau}$ . Since

Integrating out $H^\pm$
$\frac{C_{1\tau}}{m_{H^\pm}^2} \sin^2 \beta \overline{\nu_{L_i}} e_{R_i} \overline{e_L} \xi_R, \quad \frac{C_{2\tau}}{m_{H^\pm}^2} \sin^2 \beta \overline{\nu_{L_i}} e_{R_i} \overline{\mu_L} \xi_R^c, \quad \frac{C_3}{m_{H^\pm}^2} \sin^2 \beta \overline{e_L} \xi_R \overline{\xi_R^c} \mu_L$ $\frac{C_4}{m_{H^\pm}^2} \sin^2 \beta \overline{e_L} \xi_R \overline{\xi_R^c} e_L, \quad \frac{C_5}{m_{H^\pm}^2} \sin^2 \beta \overline{\mu_L} \xi_R \overline{\xi_R^c} \mu_L$
Integrating out $H$ and $A$
$\frac{C_{1\tau}}{m_H^2} \cos^2 \alpha \overline{e_i} e_i \overline{\nu_{L_e}} \xi_R, \quad \frac{C_{2\tau}}{m_H^2} \cos^2 \alpha \overline{e_i} e_i \overline{\nu_{L_\mu}} \xi_R^c, \quad C_3 \left( \frac{\cos^2 \alpha}{m_H^2} - \frac{\sin^2 \alpha}{m_A^2} \right) \overline{\nu_{L_e}} \xi_R \overline{\nu_{L_\mu}} \xi_R^c,$ $C_4 \left( \frac{\cos^2 \alpha}{m_H^2} + \frac{\sin^2 \alpha}{m_A^2} \right) \overline{\nu_{L_e}} \xi_R \overline{\nu_{L_e}} \xi_R, \quad C_5 \left( \frac{\cos^2 \alpha}{m_H^2} + \frac{\sin^2 \alpha}{m_A^2} \right) \overline{\nu_{L_\mu}} \xi_R^c \overline{\nu_{L_\mu}} \xi_R^c,$ $\frac{C_{1\tau}}{m_A^2} \sin^2 \beta \overline{e_i} \gamma_5 e_i \overline{\nu_{L_e}} \xi_R, \quad \frac{C_{2\tau}}{m_A^2} \sin^2 \beta \overline{e_i} \gamma_5 e_i \overline{\nu_{L_\mu}} \xi_R^c, \quad C_3 \left( \frac{\cos^2 \alpha}{m_H^2} - \frac{\sin^2 \alpha}{m_A^2} \right) \overline{\xi_R} \nu_{L_e} \overline{\nu_{L_\mu}} \xi_R^c,$ $C_4 \left( \frac{\cos^2 \alpha}{m_H^2} - \frac{\sin^2 \alpha}{m_A^2} \right) \overline{\nu_{L_e}} \xi_R \overline{\xi_R} \nu_{L_e}, \quad C_5 \left( \frac{\cos^2 \alpha}{m_H^2} - \frac{\sin^2 \alpha}{m_A^2} \right) \overline{\nu_{L_\mu}} \xi_R^c \overline{\xi_R^c} \nu_{L_\mu}$

**Table 2.** Effective four-Fermi operators obtained by integrating out the heavier Higgs bosons. The coefficients can be identified with Yukawa interactions as  $C_{1i} = y_{1i} y_4$ ,  $C_{2i} = y_{1i} y_5$ ,  $C_3 = y_4 y_5$ ,  $C_4 = y_4^2$  and  $C_5 = y_5^2$  with  $i = \{e, \mu, \tau\}$ .

both  $C_{1\tau}$  and  $C_{2\tau}$  have similar roles to play in our analysis and for simplicity we have assumed  $C_{1\tau} = C_{2\tau}$ . We further define  $C_\tau = \frac{C_{1\tau} \sin^2 \beta}{\Lambda^2}$ .

By the same token, after integrating out  $S$  from the last two terms of Eq. (2.1), we obtain the following four-Fermi operators which are responsible for the conversion processes inside the DS<sup>1</sup>:

$$\frac{\lambda_1}{m_S^2} \overline{\xi} \chi \overline{\xi} \xi^c, \quad \frac{\lambda_2}{m_S^2} \overline{\chi} \chi \overline{\xi} \xi, \quad (2.6)$$

where  $\lambda_1 = y_6 y_7$  and  $\lambda_2 = y_7^2$ . In this context, we would like to mention that the impact of the  $\overline{\xi} \chi \rightarrow \overline{\xi^c} \xi$  process on the dark sector freeze-out is significantly greater than that of the  $\overline{\chi} \chi \rightarrow \overline{\xi} \xi$  process unless  $\lambda_2 \gg \lambda_1$ . This issue is elaborated further in section 4.2. For the sake of simplicity a specific choice  $\lambda = \frac{\lambda_1}{\Lambda^2} = \frac{\lambda_2}{\Lambda^2}$ . Note that the first operator in Eq. (2.6) induces tree level decay of  $\chi \rightarrow 3\xi$ . In order to stop such decay kinematically, thus ensuring the stability of the DM, we impose the condition  $m_\xi < m_\chi < 3m_\xi$  in our subsequent analogy.

We thus end up with the following set of free parameters that control the DM phenomenology in the scenario under discussion:

$$\{C_\tau, m_\xi, \lambda, m_\chi\}. \quad (2.7)$$

### 3 A brief note on non-standard cosmology

According to the standard description of cosmology, the Universe is radiation-dominated in the pre-BBN era. However, the lack of direct or indirect experimental evidence keeps the possibilities

<sup>1</sup>In order to develop the effective theory we have integrated out various mass scales at different stages, however for convenience in this work we have assumed the presence of an uniform cut-off scale considering the limit  $\Lambda \simeq m_h, m_{H^\pm}, m_S$ .

of a non-standard cosmological phase in the pre-BBN era open. This means that the pre-BBN Universe could have been occupied by a fluid which red-shifting differently than the conventional radiation component. Earlier works [44–47] have reported that consideration of such a modified cosmology have non-trivial consequences on the DM phenomenology and detection prospects of the DM.

A non-standard Universe is described by the presence of a fluid having the equation of state ( $p = \omega\rho$ ) parameter  $\omega \neq \frac{1}{3}$ . If the new fluid (identified by  $\eta$ ) dominates the energy budget, the Universe goes through an expansion phase, faster than the one with the radiation component only. As a specific case study, we parameterize the energy density of the new fluid by  $\rho_\eta \propto a^{-3(1+\omega)}$  [44] which boils down to  $\rho_\eta \propto a^{-(4+n)}$  with  $\omega = \frac{1}{3}(n+1)$  and  $n > 0$ . The parameter  $n$  can take different values depending on the potential structure of  $\eta$  at the early Universe cosmology before the onset of BBN. Such modified description of the Universe requires a redefinition of the Hubble parameter ( $\mathcal{H}$ ) as given by,

$$\mathcal{H}^2 = \frac{8\pi(\rho_R + \rho_\eta)}{3M_P^2}, \quad (3.1)$$

where  $M_P = 1.22 \times 10^{19}$  GeV is the Planck mass,  $\rho_R$  and  $\rho_\eta$  correspond to the energy densities of the radiation and  $\eta$ -component, respectively. In case of secluded DS scenario  $\rho_R$  has two components,  $\rho_R = \rho_{\text{VS}}(T) + \rho_{\text{DS}}(T_D)$ , where  $T$  and  $T_D$  are temperatures of the VS and the DS, respectively. In this work we are stick to the scenario, where  $T_D \ll T$ . Thus,  $\rho_R \simeq \rho_{\text{VS}}(T)$ . The total energy density of the Universe in presence of  $\eta$ , as function of temperature, is given by,

$$\begin{aligned} \rho(T) &= \rho_R(T) + \rho_\eta(T) \\ &= \rho_R(T) \left[ 1 + \frac{g_*(T_r)}{g_*(T)} \left( \frac{g_{*s}(T)}{g_{*s}(T_r)} \right)^{(4+n)/3} \left( \frac{T}{T_r} \right)^n \right], \end{aligned} \quad (3.2)$$

where  $\rho_R = \frac{\pi^2}{30}g_*(T)T^4$  with  $g_*$  standing for the number of energy density relativistic degrees of freedom. The relativistic entropy degrees of freedom is denoted by  $g_{*s}$ . We assume that the non-standard  $\eta$  domination ends at a temperature  $T_r$ , which needs to be larger than  $T_{\text{BBN}}$  in order to keep the success of the BBN preserved. In fact, the BBN observation on the number of relativistic degrees of freedom imposes a lower bound on  $T_r$  given by  $T_r \gtrsim (15.4)^{1/n}$  MeV [44]. At very high temperature, when  $T \gg T_r$ ,  $\mathcal{H}(T)$  can be approximated as [33],

$$\mathcal{H}(T) \simeq \frac{\pi}{3M_{\text{Pl}}} \sqrt{\frac{4\pi}{5}} \sqrt{g_\rho(T)} T^2 \left( \frac{T}{T_r} \right)^{n/2}. \quad (3.3)$$

A specific case  $n = 2$  (i.e.  $\omega = 1$ ) is known as the kination phase which can be described by a scalar field whose kinetic energy dominates over the potential energy. Such an epoch normally appears in the post-inflationary phase with a steep potential [48, 49]. In our numerical analysis, we plan to put forward a comparative study on the freeze-out dynamics of secluded DM by considering both standard and non-standard cosmologies ( $n = 1$ ).

## 4 Studying the Boltzmann equations

In this section we discuss in detail the Boltzmann equations that control the dynamics of time-evolution of the number density of the DS particles. We shall also provide an analytical understanding of the equations in the subsequent subsections.

#### 4.1 Formulation of the Boltzmann equations

As stated earlier, the DS is decoupled from the VS bath and comprises of the fields  $\xi$  and  $\chi$ . Initially,  $\xi$  is produced non-thermally from the VS mainly from the processes  $\text{SM} + \text{SM} \rightarrow \xi + \text{SM}$ . As discussed earlier in section 2, the effective operators associated with  $\tau$  leptons play the dominant role in populating the DS. The contributing processes can be listed in two categories as follows:

- those proceeding via operators obtained by integrating out heavy  $H^\pm$  :

$$\begin{aligned} \bar{\tau}_R \nu_\tau &\rightarrow \bar{e}_L \xi_R, & \bar{\tau}_R e_L &\rightarrow \bar{\nu}_\tau \xi_R, & e_L \nu_\tau &\rightarrow \tau_R \xi_R, & \bar{e}_L \bar{\nu}_\tau &\rightarrow \bar{\tau}_R \bar{\xi}_R, & (+ \text{h.c.}), \\ \bar{\tau}_R \nu_\tau &\rightarrow \bar{\mu}_L \xi_R^c, & \bar{\tau}_R \mu_L &\rightarrow \bar{\nu}_\tau \xi_R^c, & \mu_L \nu_\tau &\rightarrow \tau_R \xi_R^c, & \bar{\mu}_L \bar{\nu}_\tau &\rightarrow \bar{\tau}_R \bar{\xi}_R^c, & (+ \text{h.c.}), \end{aligned} \quad (4.1)$$

- those proceeding via operators obtained by integrating out heavy  $H, A$  :

$$\begin{aligned} \bar{\tau} \tau &\rightarrow \bar{\nu}_e \xi_R, & \bar{\tau} \nu_e &\rightarrow \bar{\tau} \xi_R, & \tau \nu_e &\rightarrow \tau \xi_R, & \bar{\tau} \bar{\nu}_e &\rightarrow \bar{\tau} \bar{\xi}_R, & (+ \text{h.c.}), \\ \bar{\tau} \tau &\rightarrow \bar{\nu}_\mu \xi_R^c, & \bar{\tau} \nu_\mu &\rightarrow \bar{\tau} \xi_R^c, & \tau \nu_\mu &\rightarrow \tau \xi_R^c, & \bar{\tau} \bar{\nu}_\mu &\rightarrow \bar{\tau} \bar{\xi}_R^c, & (+ \text{h.c.}). \end{aligned} \quad (4.2)$$

Once the production of  $\xi$  is sufficient the conversion processes inside the DS *i.e.*,  $\bar{\xi}^c \xi \rightarrow \bar{\xi} \chi$  and  $\bar{\xi} \xi \rightarrow \bar{\chi} \chi$  yield  $\chi$ . When both the DS particles are coupled with significant strength with themselves and have sufficient number densities, they could reach local kinetic equilibrium with unique temperature  $T_D \neq T$  [50, 51], where  $T$  corresponds to the temperature of the VS. As discussed in section 2, the proximity in masses of these two states makes it imperative to track their individual number densities ( $n_\chi$  and  $n_\xi$ ). In addition, since the dark sector particles have a different temperature other than for the VS ones, one should also consider the evolution of the dark sector energy density ( $\rho_D = \rho_\chi + \rho_\xi$ ) as a function of  $T$ . The relevant set of Boltzmann equations with the collision term (CE) appearing in the right hand side (RHS) are as follows:

$$\begin{aligned} \frac{dn_{\chi_{\text{tot}}}}{dt} + 3\mathcal{H}n_{\chi_{\text{tot}}} &= \frac{1}{2} \langle \sigma v \rangle_{\bar{\xi}^c \xi \rightarrow \bar{\xi} \chi}^{T_D} \left[ n_{\xi_{\text{tot}}}^2 - n_{\chi_{\text{tot}}} n_{\xi_{\text{tot}}} \frac{n_{\xi_{\text{tot}}}^{\text{eq}}(T_D)}{n_{\chi_{\text{tot}}}^{\text{eq}}(T_D)} \right] \\ &+ \frac{1}{2} \langle \sigma v \rangle_{\bar{\xi} \xi \rightarrow \bar{\chi} \chi}^{T_D} \left[ n_{\xi_{\text{tot}}}^2 - n_{\chi_{\text{tot}}}^2 \frac{n_{\xi_{\text{tot}}}^{\text{eq}}(T_D)^2}{n_{\chi_{\text{tot}}}^{\text{eq}}(T_D)^2} \right], \end{aligned} \quad (4.3)$$

$$\begin{aligned} \frac{dn_{\xi_{\text{tot}}}}{dt} + \frac{dn_{\chi_{\text{tot}}}}{dt} + 3\mathcal{H}(n_{\xi_{\text{tot}}} + n_{\chi_{\text{tot}}}) &= \frac{1}{2} \left[ \langle \Gamma_{\xi \rightarrow \text{SM}} \rangle^T n_{\xi_{\text{tot}}}^{\text{eq}}(T) - \langle \Gamma_{\xi \rightarrow \text{SM}} \rangle^{T_D} n_{\xi_{\text{tot}}} \right] \\ &+ 2\gamma_{\text{SM}, \text{SM} \rightarrow \text{SM}, \xi}(T), \end{aligned} \quad (4.4)$$

$$\frac{d\rho_{D_{\text{tot}}}}{dt} + 3\mathcal{H}(\rho_{D_{\text{tot}}} + p_{D_{\text{tot}}}) = \frac{1}{2} \Gamma_{\xi \rightarrow \text{SM}} m_\xi (n_{\xi_{\text{tot}}}^{\text{eq}}(T) - n_{\xi_{\text{tot}}}) + 2\Upsilon_{\text{SM}, \text{SM} \rightarrow \text{SM}, \xi}(T), \quad (4.5)$$

where  $n_{i_{\text{tot}}} = n_{\bar{i}} + n_i$  is the total number density of the  $i^{\text{th}}$  particle with,  $n_i^{\text{eq}}(T) = \frac{g_i}{2\pi^2} m_i^2 T K_2\left(\frac{m_i}{T}\right)$ ,  $\rho_{D_{\text{tot}}} = \rho_{\bar{\chi}} + \rho_\chi + \rho_{\bar{\xi}} + \rho_\xi$  and  $p_{D_{\text{tot}}} = p_{\bar{\chi}} + p_\chi + p_{\bar{\xi}} + p_\xi$  are the total energy density and pressure of the DS, respectively. In the relativistic regime of the DS particles, the equation of state is characterized by  $p = \frac{1}{3}\rho$ , while during matter domination, it simplifies to  $p = 0$ . For the sake of simplicity, we have assumed Maxwell-Boltzmann statistics for both the  $\chi$  and  $\xi$  and express  $\rho_i$  and  $p_i$  (where

$i = \{\chi, \xi\}$  in the following form:

$$\rho_i = n_i \left( 3T_D + m_i \frac{K_1\left(\frac{m_i}{T_D}\right)}{K_2\left(\frac{m_i}{T_D}\right)} \right), \quad (4.6)$$

$$p_i = n_i T_D, \quad (4.7)$$

where,  $m_i$  is the mass of the  $i^{\text{th}}$  species and  $K_1$  and  $K_2$  are the modified Bessel functions of second kind. While deriving the Boltzmann equation, we have considered a matter-antimatter symmetry within the DS. This symmetry explains the presence of the  $\frac{1}{2}$  and 2 factors on the right-hand side (RHS) of Eqs. (4.3), (4.4) and (4.5). Once the evolution of  $\rho_D$  as function of  $T$  is known, it is possible to extract the evolution of  $T_D$  with  $T$ .

In Eq. (4.3) and Eq. (4.4),  $\langle \sigma v \rangle_{\bar{\xi}^c \xi \rightarrow \bar{\xi} \chi}^{T_D}$  and  $\langle \sigma v \rangle_{\bar{\xi} \xi \rightarrow \bar{\chi} \chi}^{T_D}$  represent the thermally averaged cross sections for the processes  $\bar{\xi}^c \xi \rightarrow \bar{\xi} \chi$  and  $\bar{\xi} \xi \rightarrow \bar{\chi} \chi$ , respectively, at temperature  $T_D$ . In Eq. (4.4)  $\langle \Gamma_{\xi \rightarrow \text{SM}} \rangle^T = \Gamma_{\xi \rightarrow \text{SM}} \frac{K_1\left(\frac{m_\xi}{T}\right)}{K_2\left(\frac{m_\xi}{T}\right)}$  refers to the thermal average of three-body decay width of  $\xi$  into the VS particles at temperature  $T$ , where  $\Gamma_{\xi \rightarrow \text{SM}}$  is the total decay width of  $\xi$ . The terms  $\gamma_{\text{SM}, \text{SM} \rightarrow \text{SM}, \xi}(T)$  in Eq. (4.4) and  $\Upsilon_{\text{SM}, \text{SM} \rightarrow \text{SM}, \xi}$  in Eq. (4.5) correspond to the collision term contributing to the production component (arising from the VS) feeding the number density and the energy density of the DS particles, respectively. The expressions for these terms are as follows:

$$\gamma_{ab \rightarrow c\xi}(T) = \frac{8\pi^2 g_a g_b T}{(2\pi)^6} \int_{s_{\min}}^{\infty} ds \lambda(s, m_c, m_\xi)^2 s^{3/2} \sigma_{c\xi \rightarrow ab}(s) K_1(\sqrt{s}/T) \quad (4.8)$$

$$\Upsilon_{ab \rightarrow c\xi}(T) = \frac{4\pi^2 g_c g_d T}{(2\pi)^6} \int_{s_{\min}}^{\infty} ds \lambda(s, m_c, m_\xi)^2 s^2 (1 - R(s, m_c, m_\xi)) \sigma_{c\xi \rightarrow ab}(s) K_2(\sqrt{s}/T) \quad (4.9)$$

Here,  $\lambda(s, m_a, m_b) = \frac{1}{2s} [(s - (m_a + m_b)^2)(s - (m_a - m_b)^2)]^{1/2}$  and  $s_{\min} = \min[(m_a + m_b)^2, (m_c + m_d)^2]$  and  $R(s, m_c, m_d) = \frac{m_d^2 - m_c^2}{s}$ . Similarly, the two terms with positive coefficients in the RHS of Eq. (4.5) serve as the source terms for the DS energy density with origins in inverse decay and scattering of SM particles, respectively, at early Universe. Due to smallness of  $T_D$ , we have safely ignored the backward reaction processes ( $\xi + \text{SM} \rightarrow \text{SM} + \text{SM}$ ) in the Boltzmann equation. The terms with a negative coefficient in the respective RHS of Eq. (4.4) and Eq. (4.5) induce the fall of  $n_\xi^{\text{tot}}$  and  $\rho_{D_{\text{tot}}}$  due to late time decay of  $\xi$ . The inclusion of the decay term for  $\xi$  in Eq. (4.4) also ensures that  $\xi$  is not sufficiently abundant in the present Universe thus establishing the present setup as a single component DM framework.

## 4.2 An analytic understanding of the Boltzmann equations

In this subsection, our aim is to comprehend Eqs. (4.3), (4.4), and (4.5) in an analytical way.

To begin with, let us concentrate on Eq. (4.5) which governs the evolution of energy density of the DS. We assume that  $\chi$  and  $\xi$  are in kinetic equilibrium after initial non-thermal production of  $\xi$  from the VS. If the coupling within the DS is not enough then  $\chi$  and  $\xi$  will not be in chemical equilibrium. This can open up the possibility of producing DM via freeze-in mechanism from  $\xi$ , which were initially produced from the VS. However, if the coupling within the DS is large enough then there exist a chemical equilibrium between  $\chi$  and  $\xi$ . Driven by the existence of the processes

within the DS, once the chemical equilibrium is attained then according to the principle of detailed balance,  $\mu_\chi = \mu_\xi = \mu_D$ , where  $\mu_\chi$  and  $\mu_\xi$  are effective chemical potential of  $\chi$  and  $\xi$ , respectively. The effect of nonzero chemical potential on DM freeze-out has been discussed in Ref. [16, 17, 52, 53]. Consequently, in such scenario, the relativistic DS particles will have an effective equilibrium number density ( $n^{\text{eq,eff}}$ ),

$$\begin{aligned} n_\chi^{\text{eq,eff}}(T) &= \frac{n_\xi(T)}{n_\xi^{\text{eq}}(T_D)} n_\chi^{\text{eq}}(T_D) \\ &= n_\chi^{\text{eq}}(T_D) e^{\frac{\mu_D}{T}}. \end{aligned} \quad (4.10)$$

To obtain an analytical estimate of  $T_D$ , we assume that  $\mu_i$  where  $i = \chi, \xi$ , is significantly smaller than the energies of the respective particles and hence can be neglected. Therefore, when the DS particles are relativistic we can write  $\rho_D = \frac{\pi^2}{30} g_{D\rho} T_D^4$ ,<sup>2</sup> where  $g_{D\rho} = g_\chi + g_\xi$  with  $g_\chi$  and  $g_\xi$  being the internal degrees of freedom for  $\chi$  and  $\xi$ , respectively. It turns out that the impact of the decay term in RHS of Eq. (4.5) at the early time of production is subdominant compared with the scattering term and can be safely ignored. We thus write  $\sigma_{\xi\text{SM}\rightarrow\text{SM},\text{SM}} \simeq \frac{C_\tau^2}{16\pi} s^3$  in the limit  $\sqrt{s} \gg m_{\chi,\xi}$  where,  $C_\tau$  is the effective coupling of  $\xi$  with the VS particles. With these, the collision term (involving  $2 \rightarrow 2$  process) appearing in the RHS of Eq. (4.5) can be estimated as,

$$\begin{aligned} \Upsilon_{\text{SM},\text{SM}\rightarrow\text{SM}\xi}^{\text{appx}}(T) &= \frac{4\pi^2 g_a g_b T}{(2\pi)^6} \int_{s_{\text{min}}}^{\infty} ds \lambda(s, m_a, m_b)^2 s^2 \frac{C_\tau^2}{16\pi} s^3 K_2(\sqrt{s}/T), \\ &= C_\tau^2 \frac{24}{\pi^5} T^9 \end{aligned} \quad (4.11)$$

Next, we derive an approximate analytical expression for  $T_D$  (a similar approach has been adopted in ref. [28]) given by

$$\zeta(T) = \left[ \int_{T_i=\Lambda}^T dT' \frac{30 \Upsilon_{\text{SM},\text{SM}\rightarrow\text{SM}\xi}^{\text{appx}}(T')}{\pi^2 g_{*D} \mathcal{H}(T') T'^5} \right]^{1/4}, \quad (4.12)$$

where  $\zeta = \frac{T_D}{T}$  and  $T_i$  corresponds to the effective cut-off scale  $\Lambda$  of the EFT. If we consider the Universe to be radiation-dominated at the production of the DS particles, then by using Eq. (4.11) and Eq. (4.12) we arrive at,

$$T_D = \sqrt{C_\tau} T \left( \frac{80 M_P \Lambda^3}{14.94 \pi^7 g_{D*} \sqrt{g_\rho}} \right)^{1/4} \propto \sqrt{C_\tau} T \Lambda^{3/4} (M_P)^{1/4}. \quad (4.13)$$

Thus, in the early Universe, when the DS particles are relativistic,  $T_D$  turns out to be proportional to  $T$ . Such a correlation has also been reported in ref. [27]. Similarly, for  $n = 1$ , using Eqs. (4.11) and (4.12), with a modified  $\mathcal{H}$  [33] given in Eq. (3.3), one finds

$$T_D \propto \sqrt{C_\tau} T \Lambda^{5/8} T_r^{1/8}. \quad (4.14)$$

Therefore, when  $\mu_D \ll E_i$  ( $E_i$  being the energy of the  $i^{\text{th}}$  particle in the DS), for a particular value of  $T_r$ , one would find, for a fast expanding Universe  $T_D$  to be smaller than what it would have

---

<sup>2</sup>For finite values of  $\mu_i$ ,  $\rho_D$  can be expressed as  $\rho_D = \frac{\pi^2}{30} g_{D\rho} T_D^4 e^{\frac{\mu_i}{T_D}}$ .

been in a radiation-dominated Universe. On the other hand, if the DS is induced by renormalizable couplings,  $T_D$  does not redshift as radiation in early Universe [28, 33, 36] even when all the DS particles are relativistic.

Note that ‘ $\mu_D$ ’ may not be always negligible (as assumed till now). If that is the case, i.e., for  $\mu_D \neq 0$ , one also has to consider the evolution of  $\frac{\mu_D}{T_D}$  with temperature ( $T$ ). Under the circumstances to obtain an accurate description of the DS dynamics, one requires solving the coupled set of Boltzmann equations. Nevertheless, the relationship between  $T_D$  and  $T$ , as mentioned earlier (see Eqs. (4.13) and (4.14)), remains valid and this can be gleaned from the numerical results presented in section 5.

We now move on to the set of Boltzmann equations in Eqs. (4.3) and (4.4). Given that  $m_\chi \approx m_\xi$ , these two equations have to be solved simultaneously. For simplicity, let us assume  $\mu_D = 0$  and thus consider the analytical expressions for  $T_D$  in Eqs. (4.13) and (4.14), depending on the cosmology of the early Universe ( $n = 0$  and  $n = 1$ , respectively). Here, both the terms on the RHS of Eq. (4.3) would contribute to the production of DM ( $\chi$ ). Once the DS reaches a thermal equilibrium with a temperature  $T_D$ , the DS particles attain the effective equilibrium number density [16, 17]. As  $T_D$  drops below  $m_\chi$ , DM ( $\chi$ ) starts annihilating to  $\xi$  via  $\bar{\xi}\chi \rightarrow \bar{\xi}^c\xi$  and  $\bar{\chi}\chi \rightarrow \bar{\xi}\xi$ . Consequently, the number density of  $\xi$  ( $n_\xi$ ) starts increasing thus prompting an eventual freeze-in for these particles. On the other hand, the number density of DM ( $\chi$ ) decreases, while approaching a freeze-out. It is important to note that due to non-renormalizable couplings, both  $\langle\sigma_{\bar{\chi}\chi \rightarrow \bar{\xi}\xi}\rangle, \langle\sigma_{\bar{\xi}\chi \rightarrow \bar{\xi}^c\xi}\rangle \propto C_7^2 m_\chi^2$ . Notably, the contributions from both the annihilation modes to the freeze-out process, at the time of DM freeze-out (characterised by the freeze-out temperature  $T_{D_{\text{fo}}}$ ) can be understood by comparing the reaction rates of these processes, i.e.,

$$\frac{\Gamma_{\bar{\xi}\chi \rightarrow \bar{\xi}^c\xi}}{\Gamma_{\bar{\chi}\chi \rightarrow \bar{\xi}\xi}} = \frac{n_\xi(T_{D_{\text{fo}}}) \langle\sigma_{\bar{\xi}\chi \rightarrow \bar{\xi}^c\xi}\rangle}{n_\chi(T_{D_{\text{fo}}}) \langle\sigma_{\bar{\chi}\chi \rightarrow \bar{\xi}\xi}\rangle}. \quad (4.15)$$

Given that the effective operators that control these processes have similar strengths, we may consider  $\frac{\langle\sigma_{\bar{\chi}\chi \rightarrow \bar{\xi}\xi}\rangle}{\langle\sigma_{\bar{\xi}\chi \rightarrow \bar{\xi}^c\xi}\rangle} \simeq 1$ . Then, by using the condition for the so-called sudden freeze-out [1], we can arrive at  $n_\chi(T_{D_{\text{fo}}}) = n_\chi^{\text{eq}}(T_{D_{\text{fo}}})$ . On the other hand, a freeze-in production of  $\xi$  (during the DM freeze-out) implies  $n_\xi(T_{D_{\text{fo}}}) > n_{\xi_{\text{eq}}}(T_{D_{\text{fo}}})$ . Eqn. (4.15) then leads to the following relation:

$$\begin{aligned} \frac{\Gamma_{\bar{\xi}\chi \rightarrow \bar{\xi}^c\xi}}{\Gamma_{\bar{\chi}\chi \rightarrow \bar{\xi}\xi}} &> \frac{n_\xi^{\text{eq}}(T_{D_{\text{fo}}})}{n_\chi^{\text{eq}}(T_{D_{\text{fo}}})}, \\ &> \left(\frac{m_\xi}{m_\chi}\right)^{3/2} \exp\left(\frac{m_\chi - m_\xi}{m_\chi} x_{D_{\text{fo}}}\right), \end{aligned} \quad (4.16)$$

where,  $x_{D_{\text{fo}}} = \frac{m_\chi}{T_{D_{\text{fo}}}} \sim 20$ . This implies that, in our scenario, the reaction rate of  $\bar{\xi}\chi \rightarrow \bar{\xi}^c\xi$  would be much larger than that of  $\bar{\chi}\chi \rightarrow \bar{\xi}\xi$  at the time of DM freeze-out.

## 5 Results

Since, in this work we are interested in the secluded DS scenario, we first focus on the specific region of the parameter space where the DS and the VS coexist without being in a state of thermal equilibrium. Subsequently, we proceed to solve the Boltzmann equation as presented in section 4.1 and estimate the DM relic abundance in such a scenario. We have also discussed about possible constraints on model parameter space from different cosmological and astrophysical scenarios.

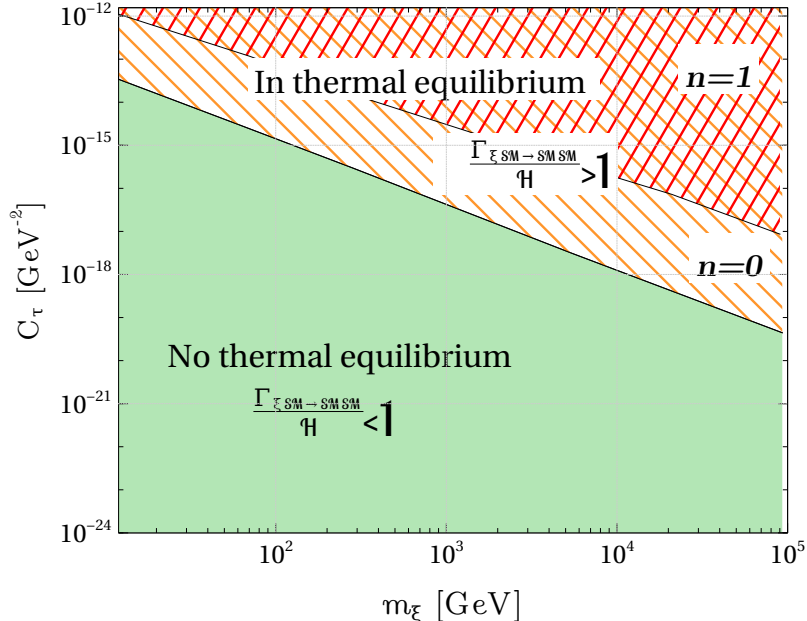


**Figure 1.** The status of a possible thermal equilibrium between the DS and the VS presented in the  $m_\xi - C_\tau$  plane for  $n = 0, 1$  with  $T = \Lambda (= 100 m_\chi)$ . See text for details.

### 5.1 The region (out) of thermal equilibrium

We identify the region of parameter space where the DS and the VS are out of thermal equilibrium by first delineating the region where these sectors are indeed in thermal equilibrium. Towards this, we follow the conventional approach that involves computation of the collective reaction rates responsible for the production of the particles belonging to the VS from the DS ones, juxtaposing those with the Hubble parameter ( $\mathcal{H}$ ). The quantity that determines whether a thermal equilibrium is established or not between the two sectors is  $\frac{\Gamma_{\xi SM \rightarrow SM SM}}{\mathcal{H}}$ , where  $\frac{\Gamma_{\xi SM \rightarrow SM SM}}{\mathcal{H}} > (<)1$  implies the equilibrium is (not) realized.

In Fig. 1, we contrast the regions in the  $m_\xi - C_\tau$  plane over which the DS and the VS could eventually move into a thermal equilibrium as opposed to where those remain out of equilibrium, the latter being the target region of the present study. The choice of the indicated plane is prompted by the fact that  $m_\xi$  and  $C_\tau$  are the two parameters that primarily control the ratio  $\frac{\Gamma_{\xi SM \rightarrow SM SM}}{\mathcal{H}}$ , the very quantity that decides, in the first place, the feasibility of a thermal equilibrium. In addition,  $m_\xi$  restricts the DM mass,  $m_\chi$ , such that the latter not only becomes stable but also could account for its observed value of relic abundance. As for  $C_\tau$ , it plays an important role in accounting for the observed relic abundance as well as a successful BBN. Furthermore, the figure is drawn for  $T = \Lambda (= 100 m_\chi)$ .

Over the checkered wedge-shaped region in red at the top of Fig. 1, the DS and the VS coexist in thermal equilibrium when  $n = 1$ . For  $n = 0$ , such a region is extended by the hashed strip in orange for  $n = 0$ . Conversely, for  $n = 0$ , the coveted region over which the two sectors would be out of thermal equilibrium is shown in light green. For  $n = 1$ , such a region now extends upwards to capture the hashed region in orange. Notably, as  $m_\xi$  increases, the reaction rates get enhanced,

which thus looks for smaller  $C_\tau$ 's for larger values of  $m_\chi$  so that the two sectors still remains out of thermal equilibrium.

At this point, it may be noted that the interactions between the DS and the VS are controlled by the dim-6 effective operators as discussed in section 2. The processes that describe the production of the VS states from the DS ones are just the reverse ones of those mentioned in Eqs. (4.1) and (4.2). The expression for the relevant collision term at very high temperatures can be obtained in the same way as has been for  $\Upsilon_{ab\rightarrow c\xi}$  in section 4.2 and is found to vary as  $\gamma_{ab\rightarrow c\xi} \propto C_\tau^2 T^8$ . Consequently, the reaction rate of  $\xi \text{ SM} \rightarrow \text{SM SM}$  processes is given by  $\Gamma_{\xi \text{ SM} \rightarrow \text{SM SM}} \propto C_\tau^2 T^5$ . Thus,  $\frac{\Gamma_{\xi \text{ SM} \rightarrow \text{SM SM}}}{\mathcal{H}}$  drops as  $T$  decreases. This signifies that a DS of a secluded kind at a higher temperature would remain so at a lower temperature.

Thus, a departure from thermal equilibrium between the DS and the VS may be allowed at a higher value of  $T (> 100 m_\chi)$  and still remain germane for the present work. However, this necessitates a smaller  $C_\tau$  to throw the DS-VS system out of equilibrium at that high temperature. As we will see later (see Fig. 5), such a smaller value of  $C_\tau$  tends to attract constraints from BBN. In other words, for our present purposes, the maximum temperature at which the DS-VS system could be thrown out of thermal equilibrium is dictated by the requirement of a successful BBN.

## 5.2 Numerical study of Boltzmann equations

The main goal of the present study is to delineate the regions of the model parameter space that conform with various cosmological and astrophysical constraints like those from the BBN and the observed relic abundance, the latter being realised either via freeze-out or through freeze-in of the DM. We consider both standard cosmology ( $n = 0$ ) and a fast(er) expanding Universe ( $n = 1$ ). We then proceed to solve the coupled set of Boltzmann equations in Eqs. (4.3), (4.4) and (4.5) numerically.

To understand the key issues like the evolution of the number densities ( $n_{\chi,\xi}$ ) of  $\chi$  and  $\xi$ , we track the evolution of the DS temperature,  $T_D$ , as a function of  $x = \frac{m_\chi}{T}$ . As mentioned before, we set the cut-off scale of the effective theory to be  $\Lambda = 100 m_\chi$ . We set  $T_r = 20 \text{ MeV}$  for  $n = 1$  (see section 3). To have a quantitative analysis of the DS dynamics, in this work, we consider two benchmark points (scenarios) with  $\{C_\tau, m_\xi, m_\chi\} \equiv \{10^{-21} \text{ GeV}^{-2}, 10^4 \text{ GeV}, 2 \times 10^4 \text{ GeV}\}$  (**BP-1**) and  $\{10^{-21} \text{ GeV}^{-2}, 5 \times 10^4 \text{ GeV}, 10^5 \text{ GeV}\}$  (**BP-2**).

To start with, we allow for  $\mu_D \neq 0$ . Hence, following discussions in section 4.2, we present in the left plot of Fig. 2 the variation of  $\frac{\mu_D}{T_D}$  with ' $x$ '. For the purpose in hand, we find it sufficient to stick to the benchmark scenario, BP-1. The dotted blue and the solid black lines illustrate such variations for  $n = 0$  and  $n = 1$ , respectively. The corresponding values of ' $\lambda$ ' that are used for the purpose are also indicated. The values are so chosen that those reproduce the DM relic abundance in the right (observed) ballpark. As the temperature ( $T$ ) of the Universe drops and the DM freezes out, the ratio  $\frac{\mu_D}{T_D}$  starts increasing, as can be seen in this plot. Notably, because of a higher expansion rate of the Universe for  $n = 1$ , the processes that produce the DS particles would decouple at an earlier time when compared to a radiation-dominated Universe, for any fixed set of values of  $C_\tau$ ,  $m_\xi$  and  $m_\chi$ . Consequently, the initial number density of non-thermally produced  $\xi$  ( $n_\xi$ ) will be smaller in this case. This drives the ratio  $\frac{\mu_D}{T_D}$  to smaller values as can be clearly seen in the left plot of Fig. 2.

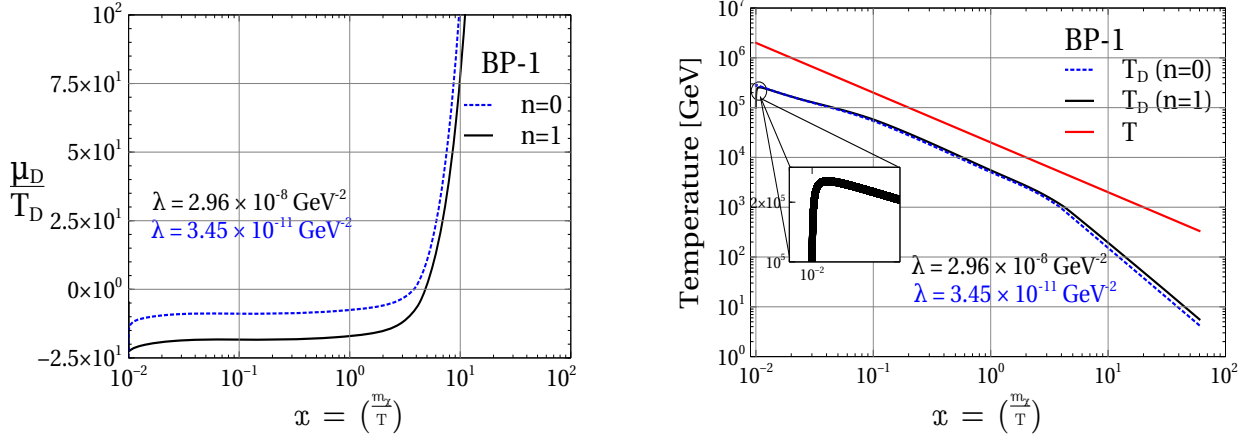


**Figure 2.** Evolution of  $\frac{\mu_D}{T_D}$  (left) and  $T_D$  (right) as a function of  $x (= m_\chi/T)$  for the scenario BP-1. Two different cosmological scenarios,  $n = 0$  (blue dashed) and  $n = 1$  (black solid) have been considered. In the right plot, the red solid line represents the evolution of  $T$  with  $x$ .

In the right panel of Fig. 2, we show the evolution of  $T_D$  and  $T$  as functions of ‘ $x$ ’. Variations of  $T_D$  are presented for two pertinent cases: the blue dashed and the black solid lines correspond to scenarios with  $n = 0$  and  $n = 1$ , respectively. The red solid line represents the evolution of  $T$ . Initially, the temperature of the hidden sector increases because of a transfer of energy from the VS bath. This is shown in the inset by zooming up the region of the curve where such an increase occurs. Subsequently, as ‘ $x$ ’ increases, the curves for  $T_D$  and  $T$  appear to turn nearly parallel to each other in such a log-log plot. This implies that, over this parallel regime,  $T_D \propto T$ , as long as the DS remains relativistic. Such a situation indeed follows from the analytical solution of  $T_D$  that we have (see equations Eqs.(4.13) and (4.14)) and as explained in section 4.2. Once  $T_D$  goes below  $m_\xi$ , it starts to red-shift like matter. Let us note in passing that in such a scenario where  $\mu_D$  cannot be ignored, the  $T_D$ ’s for a radiation-dominated Universe ( $n = 0$ ) and a fast expanding Universe ( $n = 1$ ) get to be close to each other.

In the left (right) panel of Fig. 3, we discuss the temperature evolution of the ratio,  $\Omega/\Omega_{\text{obs}}$ , for  $\chi$  and  $\xi$  (by solid and dashed lines, respectively), for both benchmark points BP-1 (BP-2). Here, the relic abundance  $\Omega$  predicted by the model is given by  $\Omega = \frac{m_\chi s_0 Y_i}{\rho_{\text{crit}}} = 2.755 \times 10^8 \left( \frac{m_i}{1 \text{ GeV}} \right) Y_i(T)$ ,  $i \ni \chi, \xi$  with  $Y_i(T) = \frac{n_i(T)}{s(T)}$ , where  $s(T)$  is the entropy density of the Universe while ‘ $\Omega_{\text{obs}}$ ’ is the observed DM relic abundance. Curves in red and blue stand for different sets of values of ‘ $\lambda$ ’ which give rise to two distinct mechanisms of DM production in the DS, i.e., freeze-out (larger ‘ $\lambda$ ’) and freeze-in (smaller ‘ $\lambda$ ’), respectively. Next, we estimate the required value of ‘ $\lambda$ ’ for each benchmark point such that we obtain the observed (within  $1\sigma$ ) DM relic abundance, i.e.,  $0.118 \leq \Omega_{\text{obs}} \leq 0.121$ , considering an radiation-dominated cosmology ( $n = 0$ ). At an early time, both  $\xi$  and  $\chi$  have vanishing initial abundance. However, over time, their co-moving number densities ( $Y_{\chi,\xi}$ ) gradually increase as can be seen in this figure.

For the larger values of ‘ $\lambda$ ’ in these two plots (in red, with  $\lambda = 3.45 \times 10^{-11} \text{ GeV}^{-2}$  and  $\lambda = 4.322 \times 10^{-13} \text{ GeV}^{-2}$ , respectively), there exists a chemical equilibrium between  $\chi$  and  $\xi$ .

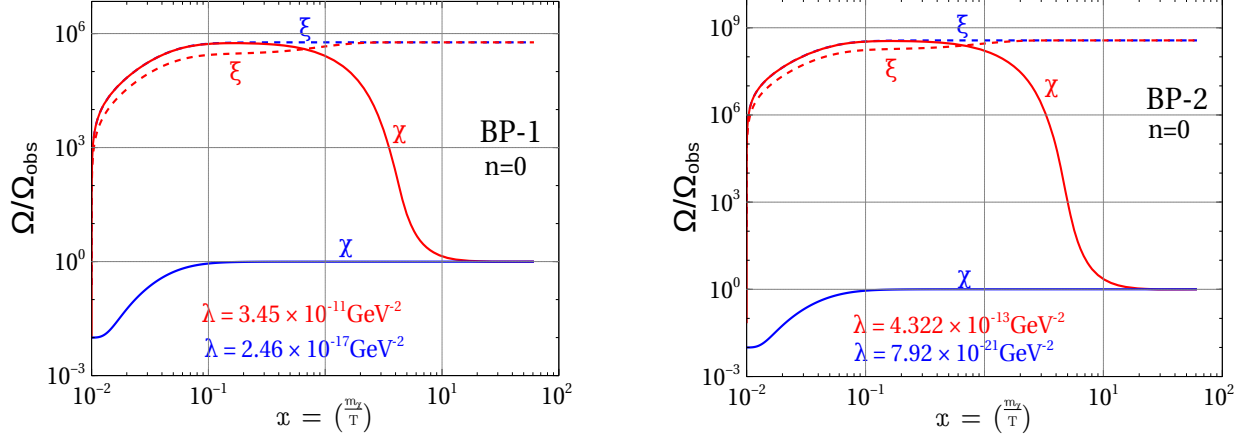


**Figure 3.** Evolution of  $\frac{\Omega}{\Omega_{\text{obs}}}$  as a function of  $x(= m_\chi/T)$  for  $\chi$  (solid) and  $\xi$  (dashed) for scenarios BP-1 (left) and BP-2 (right) with  $n = 0$  cosmology. Results for both freeze-out (red) and freeze-in (blue) scenarios are shown.

When the DS temperature  $T_D$  becomes comparable to  $m_\chi$ ,  $\chi$  annihilates to  $\xi$  dominantly through the process  $\bar{\xi}\chi \rightarrow \bar{\xi}^c\xi$  as elaborated in section 4.2. Finally, when the reaction rate of this particular process drops below  $\mathcal{H}$ , the DM freezes out. Consequently, the comoving number density of  $\xi$  ( $Y_\xi$ ) increases and, eventually,  $\xi$  ‘freezes in’. In contrast, for the smaller values of the ‘ $\lambda$ ’ (in blue, with  $2.46 \times 10^{-17} \text{ GeV}^{-2}$  and  $\lambda = 7.92 \times 10^{-21} \text{ GeV}^{-2}$ , respectively), the DS is unable to reach a chemical equilibrium because of an insufficient interaction rate inside the DS. Thus, in this case, the correct DM relic abundance can only be achieved via the freeze-in mechanism.

Further, we point out that, for the benchmark scenario BP-2 (the plot on the right), one requires a lower value of ‘ $\lambda$ ’; be it a freeze-out or a freeze-in mechanism at play, when compared to what is required in BP-1 (the plot on the left) having same value of  $C_\tau$ . This could be understood by noting that in the presence of non-renormalizable couplings in the DS, the thermally averaged cross-section for the process  $\bar{\xi}\chi \rightarrow \bar{\xi}^c\xi$  increases with the mass of the DM particle ( $m_\chi$ ), in contrast to what happens when dealing with renormalizable couplings. Hence the scenario BP-2 requires a smaller interaction rate (and hence a smaller ‘ $\lambda$ ’) to reach the right abundance.

In Fig. 4, we present the results of a same exercise as done for Fig. 3, but now in a non-standard cosmological scenario with  $n = 1$  and  $T_r = 20 \text{ MeV}$  (as mentioned earlier). Such a fast expanding Universe implies an early decoupling of the DM from the DS thermal bath. As may be expected, this results in an overabundance of the DM when ‘ $\lambda$ ’ is of the same order as used in Fig. 3. Hence, for DM freeze-out, one now requires a much larger (by a few orders) value of ‘ $\lambda$ ’ when compared to what would be needed in a radiation-dominated Universe, for both BP-1 and BP-2. This feature would generally boost the DM indirect search cross section as discussed in detail in section 5.4. Similarly, in case of DM freeze-in, we also need a somewhat larger ‘ $\lambda$ ’ in order to obtain the relic abundance in the right ballpark.

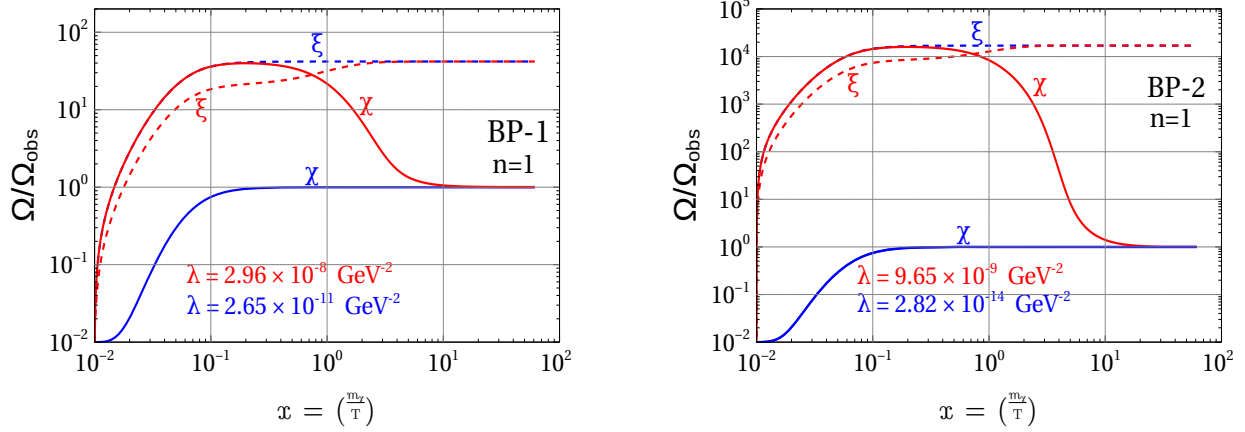


Figure 4. Same as in Fig. 3 but with  $n = 1$ .

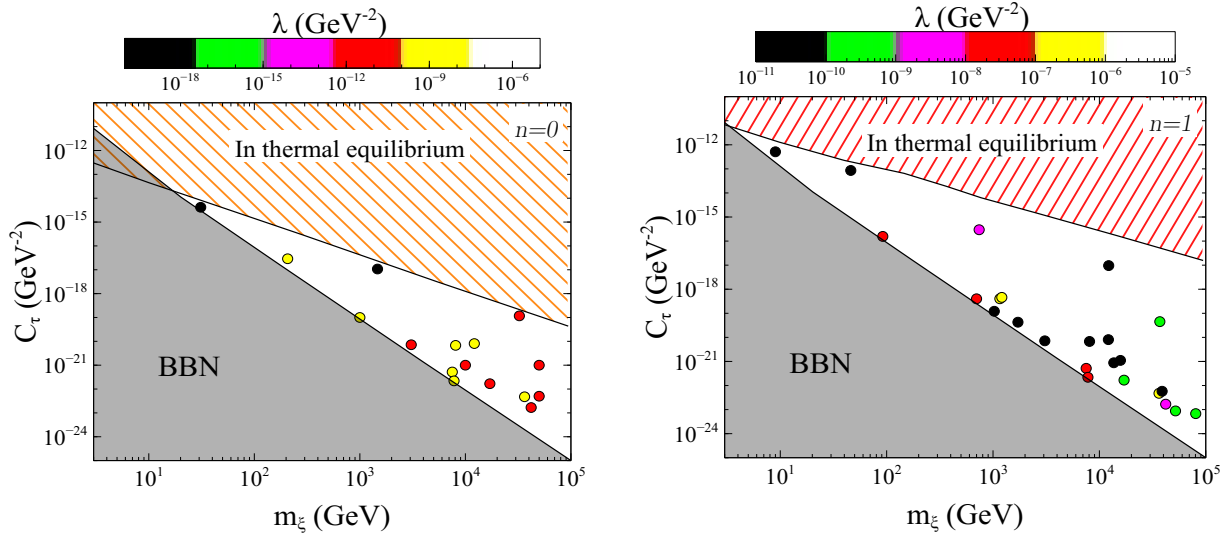
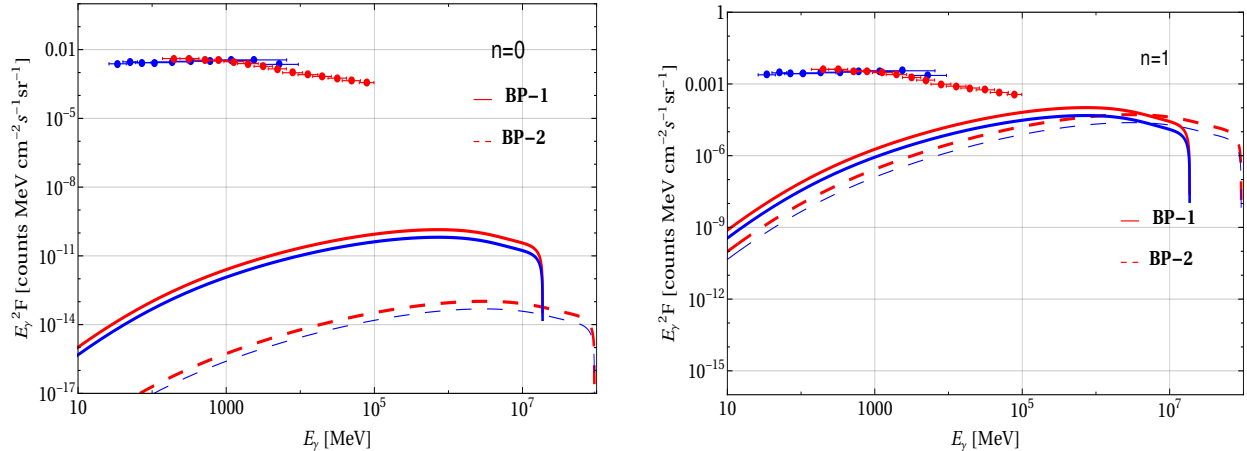


Figure 5. Regions in the  $m_\xi - C_\tau$  plane that are constrained by requiring a successful BBN (in gray), that leaves the DS and the VS in thermal equilibrium (hashed in orange ( $n = 0$ ) and red ( $n = 1$ )), the left over (coveted) region (the white wedge) which is compatible with a successful BBN while having the DS and the VS off thermal equilibrium. Colored points scattered over the white wedge represent parameter values which, in addition, comply with the observed DM relic abundance, the colors being indicative of the values of ‘ $\lambda$ ’ as shown in the palette.

### 5.3 Constraints from the Big Bang Nucleosynthesis

In the standard picture of Big-Bang Nucleosynthesis (BBN), around temperature  $\lesssim \mathcal{O}(1)$  MeV, the energy of the cosmic microwave background (CMB) photons becomes lower than the binding energies of the light elements, e.g., deuterium (D),  $^3\text{He}$ ,  $^4\text{He}$ ,  $^7\text{Li}$  and hence these elements/isotopes get synthesized [54]. There are strict observational constraints on the primordial abundances of these light elements (see section 2 of reference [55] and references therein). If a long-lived particle is produced in the early Universe and it decays subsequently into SM particles at late time, the BBN



**Figure 6.** Variation of differential photon flux,  $E_\gamma^2 F$  (where  $F = \frac{d\Phi}{dE_\gamma}$ ) as a function of  $E_\gamma$  for BP-1 (solid) and BP-2 (dashed), considering both  $n = 0$  (left) and  $n = 1$  (right) cosmology. In the top part of each plot shown are the data points from the Fermi-LAT [38, 39] (in red) and the EGRET [60, 61] (in blue) experiments.

predictions might get altered. Thus, given that the relevant observables have now been precisely measured, such an effect can be used to constrain the model parameters.

In our framework, the state  $\xi$  is unstable and can be long-lived depending on the smallness of the coupling coefficient  $C_\tau$ . Once the DS freezes out or freezes in,  $\xi$  finally decays to the SM leptons. If such decays occur during the BBN, the newly produced charged leptons could emit energetic photons (electromagnetic shower) which, in turn, could interact with the CMBR photons and trigger photo-dissociation process [55–58] thus altering the abundance of light elements. On the other hand, high energy neutrinos that might appear from such decays could scatter off the background leptons and produce charged leptons and charged pions. The former could, once again, induce electromagnetic showers that might destroy light elements that are already synthesized while the latter impacts the  $n - p$  ratio through nucleon and pion interactions [59]. In view of these and hence in order to evade any significant impact on the outcome of BBN, it is apparently safe to make  $\xi$  decays early enough with  $\tau_\xi > 1$  second, which translates to  $T < 3$  MeV.

As discussed in section 5.1, with increasing  $m_\xi$ ,  $C_\tau$  has to drop if the DS and the VS have to remain out of thermal equilibrium. Also, as can be gleaned from Fig. 1, for  $n = 1$ , an off-equilibrium situation can be realized over a larger region of parameter space thanks to the faster expansion of the Universe. In Fig 5, we highlight the region (gray-shaded) where the smallness of  $C_\tau$  makes  $\xi$  decay at a later time, i.e, at a temperature below 3 MeV, thus affecting a successful BBN. The two aforesaid constraints, in conjunction, put a lower bound on  $m_\xi$  and exclude  $m_\xi < 20$  GeV for  $n = 0$  (left plot) and  $m_\xi < 2$  GeV for  $n = 1$  (right plot). We also show a few points in the parameter space spanned by  $m_\xi$ ,  $C_\tau$  and  $\lambda$  for which the DM relic abundance turns out to be in the right ballpark. Note that these points carry different values for  $m_\chi$  as  $m_\xi$  changes. It thus appears that the coveted region of parameter space where the DS and the VS are going to be off-equilibrium could give rise to the observed DM relic abundance for both  $n = 0$  and  $n = 1$  cosmologies.

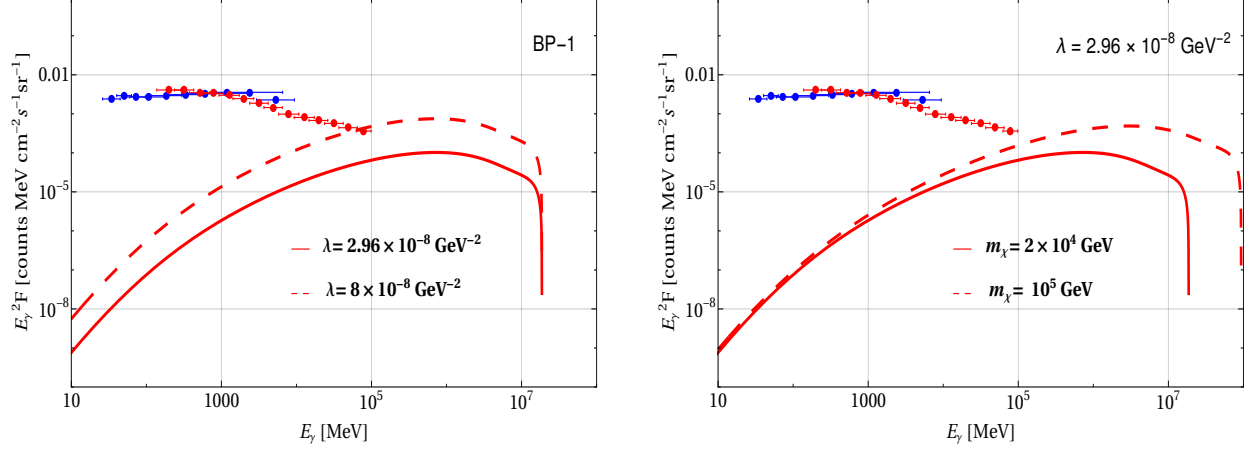


**Figure 7.** Same as in Fig. 6 but for varying  $\lambda$  (left, with fixed  $m_\chi$  as in BP-1), and  $m_\chi$  (right, with fixed  $\lambda$ ).

#### 5.4 Indirect detection of the DM in gamma ray searches

In the scenario presented in this work, prompt photons ( $\gamma$ ) can be generated from one-step cascades of a pair of  $\xi$ 's produced in the mutual annihilation of the DM particles. Schematically, this is given by  $\bar{\chi}\chi \rightarrow \bar{\xi}\xi$ , followed by  $\xi_R \rightarrow \bar{\tau}_R \nu_\tau e_L$ ,  $\xi_R^c \rightarrow \bar{\tau}_R \nu_\tau \mu_L$ , where the prompt photons have their origins in the QED and electroweak bremsstrahlung off the charged leptons. The differential photon flux originating from such a cascade is given by [62–64]

$$\frac{d\Phi}{dE_\gamma \Delta\Omega} = \frac{\langle\sigma v\rangle_{\bar{\chi}\chi \rightarrow \bar{\xi}\xi}}{16\pi m_\chi^2} \rho_\odot^2 R_\odot \bar{J}_{\text{ann}} \sum_l \text{Br}(\xi \rightarrow l + \nu) \frac{dN_\gamma^l}{dE_\gamma}, \quad (5.1)$$

where  $\langle\sigma v\rangle_{\bar{\chi}\chi \rightarrow \bar{\xi}\xi}$ ,  $\text{Br}(\xi \rightarrow l + \nu)$  and  $m_\chi$  are the model-dependent quantities. Here, we have adopted the Navarro–Frenk–White (NFW) density profile for the DM [65, 66] which sets the DM mass-density  $\rho_\odot = 0.3 \text{ GeV} \cdot \text{cm}^{-3}$  at the solar location while  $R_\odot$  is the distance vector between the galactic center and the Sun. The term  $\bar{J}_{\text{ann}}$  is completely determined by the distribution of the DM mass density  $\rho(r)$  and is defined as,

$$\bar{J}_{\text{ann}} = \frac{1}{\Delta\Omega} \int d\Omega \int \frac{d\ell}{R_\odot} \left( \frac{\rho[r(\ell, \psi)]}{\rho_\odot} \right)^2 \quad (5.2)$$

where ‘ $r$ ’ is the distance of the source under survey from the galactic center,  $\ell$  is its distance from the observer along the line of sight,  $\psi$  is the angle between the line of sight and  $R_\odot$ ,  $\text{Br}(\xi \rightarrow l + \nu)$  is the relevant decay branching fractions of  $\xi$  to charged leptons. The quantity  $\frac{dN_\gamma^l}{dE_\gamma}$ , i.e., the photon energy spectrum is obtained by using the publicly available package PPPC4DMID [67].

We now move on to study the relevant photon spectra numerically and to check how those compare with the latest experimental results (limits) from various experiments (like Fermi-LAT [38, 39], EGRET [60, 61], in particular) that carries out indirect searches for the DM. In Fig 6, we present the energy spectra of photon flux for the scenarios BP-1 (solid lines) and BP-2 (dashed

lines) which are projected (at the bottom) for the experiments Fermi-LAT (red) and EGRET (blue) and compare them with the corresponding experimental results (at the top). The left (right) plot refers to  $n = 0$  ( $n = 1$ ) where the values of ‘ $\lambda$ ’ that we use are those obtained for the freeze-out scenarios in Fig 3 and Fig. 4 (shown there in red). In the left plot ( $n = 0$ ), we observe that in both the scenarios BP-1 and BP-2, the photon flux remains far below the level of current sensitivity of both Fermi-LAT and EGRET over the relevant range of  $E_\gamma$ . This is because of the smallness of ‘ $\lambda$ ’ which is required to conform with the observed DM relic abundance. However, from the right plot where we present the case of  $n = 1$ , i.e., that of a faster expanding Universe, one finds that the photon fluxes are increased for the same benchmark points. This is since, as discussed in section 5.2 a faster expanding Universe requires larger values of ‘ $\lambda$ ’ to find the DM relic abundance in the right ballpark. Such a scenario could thus have an enhanced sensitivity to the DM indirect search experiments.

Thus, in Fig. 7 we set  $n = 1$  and present how the sensitivity to experiments could get further enhanced. Towards this, we study the energy spectrum of the photon flux as a function of  $\lambda$  (left plot) and  $m_\chi$  (right plot). We pick BP-1 as the reference scenario for this study since, as can be seen from Fig. 6, results in a larger flux when compared to BP-2. It may then be noted that while varying  $\lambda$  in the left plot, one can still stick to the scenario BP-1 given the way it is defined. However, varying  $m_\chi$ , as is done in the right plot, necessarily leads to a departure from BP-1.

In the left plot of Fig. 7, we have thus compared the energy spectra of the photon flux for the scenario BP-1 with two different values of  $\lambda$ :  $\lambda = 2.96 \times 10^{-8} \text{ GeV}^{-2}$  (red solid line) and  $\lambda = 8 \times 10^{-8} \text{ GeV}^{-2}$  (red dashed line). Note that the value  $\lambda = 2.96 \times 10^{-8} \text{ GeV}^{-2}$  has already been indicated (see the left plot of Fig.4) to give rise to the observed relic abundance. The present plot thus demonstrates how an increased  $\lambda$  could bring the photon flux within the reach of the more sensitive experiment, i.e. Fermi-LAT. This can be traced to the fact that, with increasing ‘ $\lambda$ ’,  $\langle\sigma v\rangle_{\bar{\chi}\chi\rightarrow\bar{\xi}\xi}$  increases which, in turn, pushes up the photon spectra (see Eq.5.1). However, for such larger values of ‘ $\lambda$ ’, the DM would annihilate rapidly thus leading to its under abundance. Nonetheless, one could still get back the right abundance if a larger value of ‘ $n$ ’ ( $> 1$ ) can be used. In the right panel of Fig. 7 we present the energy spectra of photon flux for two different values of  $m_\chi$ :  $m_\chi = 2 \times 10^4 \text{ GeV}$  (red solid line) and  $m_\chi = 10^5 \text{ GeV}$  (red dashed line)<sup>3</sup> with the same coupling strength  $\lambda = 2.96 \times 10^{-8} \text{ GeV}^{-2}$ . It is evident from this plot that as  $m_\chi$  increases, photon flux also increases. This is because of the nature of the dim-6 operators obtained by integrating out the heavy mediator  $S$  in the process  $\bar{\chi}\chi \rightarrow \bar{\xi}\xi$  (see section 4.2) that makes  $\langle\sigma v\rangle_{\bar{\chi}\chi\rightarrow\bar{\xi}\xi}$  increase with  $m_\chi$ . Note that even for the larger value of  $m_\chi$  that we use in the plot is nearly the maximum one that can be handled by the package PPPC4DMID the photon spectrum remains below the current Fermi-LAT sensitivity. As for the DM relic abundance, an enhanced  $m_\chi$  again leads to its under abundance, for reasons discussed earlier (see section 5.2) and as for the plot in left  $n > 1$  could help back getting back the observed relic abundance of the DM.

In Fig. 8, we present how the Fermi-LAT [38, 39] results restrict the  $m_\chi - \lambda$  plane. To find this out, we perform a small scan over the parameters  $\{\lambda, m_\chi\}$  while setting  $m_\xi = \frac{m_\chi}{2}$ . For some given sets of values for  $\{m_\chi, \lambda\}$ <sup>4</sup>, we then estimate the differential photon flux, as presented in Eq.(5.1), as a function of ‘ $E_\gamma$ ’ and ensure that the value of the flux thus obtained does not exceed

<sup>3</sup>Varying  $m_\chi$  necessarily alters  $m_\xi$ .

<sup>4</sup>The differential photon flux is proportional to  $\text{Br}(\xi \rightarrow l + \nu)$  as in Eq.(5.1) and hence insensitive to changing  $C_\tau$ .

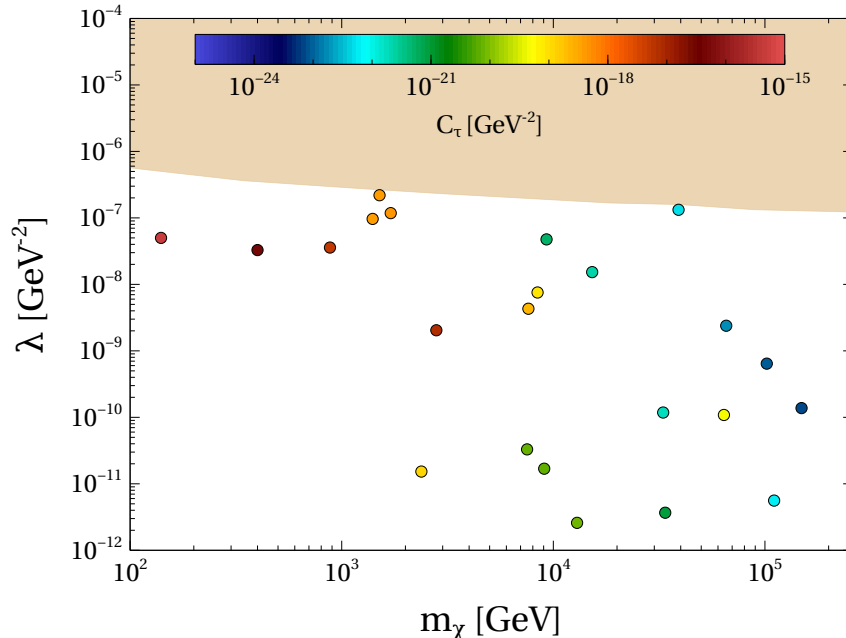


**Figure 8.** Region in the  $m_\chi - \lambda$  plane (in light-brown) excluded by the Fermi-LAT [38, 39] data. Scattered dots are the relic satisfied points with different colors representing required order of magnitude for  $C_\tau$ .

its upper bound as set by Fermi-LAT [38, 39]. This then rules out a region in the  $m_\chi - \lambda$  plane which is delineated in the figure in light-brown shade. The colored dots represent points in the parameter space that yield DM relic abundance within the observed ballpark, the associated colors being indicators of the required order of magnitude of  $C_\tau$  (for a particular set of  $\{m_\chi, \lambda\}$ ) as can be gleaned from the palette.

## 6 Summary and Conclusions

In this work, we present an effective field theory motivated description of secluded dark matter and discuss its phenomenological implications in the light of a radiation-dominated ( $n = 0$ ) and a fast expanding ( $n = 1$ ) Universe. As a viable UV-complete framework, we have explored the type-X 2HDM extended by two fermionic fields,  $\chi$  and  $\xi$ , and one scalar field  $S$  all belonging to a secluded dark sector along with a global  $U(1)_{e-\mu}$  symmetry. The choice of such a UV scenario is guided by the possibilities that it offers for the initial non-thermal production of the dark sector particles,  $\xi$  and  $\chi$ , from the visible sector and those for the conversion processes of the dark sector particles, along with different astrophysical (indirect detection of  $\gamma$ -ray spectra) and cosmological observations (BBN).

We then construct various dim-6 four-Fermi operators by integrating out the heavier Higgs bosons ( $H^\pm$ ,  $H$  and  $A$ ) and the heavy dark sector scalar excitation,  $S$ . These operators control the interactions between the dark sector and the visible sector particles as well as the interactions involving only the dark sector particle,  $\chi$  and  $\xi$ . Primarily, we have identified the regions in the  $(m_\xi - C_\tau)$  plane where the two sectors are not in thermal equilibrium for both the cosmological

setup. This leads to the requirement of a smaller value of the portal coupling ( $C_\tau$ ). Equipped with this we have carried out a comprehensive numerical analysis by solving the appropriate set of coupled Boltzmann equations after incorporating all relevant production and annihilation processes of the dark matter ( $\chi$ ) and the mediator ( $\xi$ ) particles.

The salient observations that can be made from the present analysis are as follows.

- The proposed framework enables the determination of can explain the observed DM relic abundance either via freeze-out or through freeze-in in the dark sector depending on the strength of the interactions between  $\chi$  and  $\xi$ . When a freeze-out is at play, we find that the process  $\bar{\xi}\chi \rightarrow \bar{\xi}^c\xi$  plays a dominant role in DM freeze-out in the dark sector as compared to the process  $\bar{\chi}\chi \rightarrow \bar{\xi}\xi$ .
- The effective four-Fermi interactions between the visible and the dark sector lead to the proportionality of dark sector temperature ( $T_D$ ) and the visible sector temperature ( $T$ ) at an epoch when the dark sector particles are relativistic. As a result, we find that relatively smaller values of ‘ $\lambda$ ’ are preferred for an increasing mass of the dark matter ( $m_\chi$ ) in order to conform with the observed DM relic abundance.
- For  $n = 1$  (i.e., the fast expanding Universe), one requires larger values of ‘ $\lambda$ ’ (for a fixed set of values of  $m_\chi$  and  $C_\tau$ ) compared to the ones needed when  $n = 0$  to find the DM relic abundance at the right ballpark. This results in an enhanced gamma-ray flux in such a scenario resulting from DM annihilation and thus brings it closer to the current limit of sensitivity of the Fermi-LAT experiment. It also suggests that cosmological scenarios with  $n > 1$  (requiring a further larger ‘ $\lambda$ ’) are likely to be restricted by the Fermi-LAT data.
- The portal coupling,  $C_\tau$ , is required to be on the smaller side to keep the dark sector out of thermal equilibrium. However, a small  $C_\tau$  makes the dark sector excitation  $\xi$  long-lived which can potentially ruin the success of BBN. As a result,  $m_\xi < 20$  GeV region is disfavored for  $n = 0$ , while for  $n = 1$ , the situation gets somewhat relaxed as only the region with  $m_\xi < 2$  GeV turns out to be disallowed.

Hence, for  $n = 1$ , i.e, a fast expanding Universe, one ends up with a larger volume of allowed parameter space which conforms with all relevant constraints coming from the BBN, the requirement of having the dark and the visible sectors to be off equilibrium and the observed DM relic abundance.

Exploring the phenomenological implications of an EFT motivated secluded dark matter scenario with dim-6 operators has been the main objective of the present work. The observations made here are mostly generic and are expected to hold in possible alternate BSM theories, effectively resulting into to a secluded dark matter scenario, the dynamics of which is regulated by various dim-6 operators. In this context, choice of a different global symmetry other than  $U(1)_{e-\mu}$  may also be considered. Regarding the BBN constraints, some improvement of our analysis is still possible, by performing a precise computation of abundances of primordial elements in the presence of decays of a long-lived  $\xi$ . We leave such studies for a future work.

## 7 Acknowledgement

AKS is supported by a postdoctoral fellowship at IOP, Bhubaneswar, India. AT would like to acknowledge the financial support provided by the Indian Association for the Cultivation of Science (IACS), Kolkata.

## References

- [1] Y. Sofue and V. Rubin, *Rotation curves of spiral galaxies*, *Ann. Rev. Astron. Astrophys.* **39** (2001) 137 [[astro-ph/0010594](#)].
- [2] D. Clowe, A. Gonzalez and M. Markevitch, *Weak lensing mass reconstruction of the interacting cluster 1E0657-558: Direct evidence for the existence of dark matter*, *Astrophys. J.* **604** (2004) 596 [[astro-ph/0312273](#)].
- [3] D. Clowe, M. Bradac, A. H. Gonzalez, M. Markevitch, S. W. Randall, C. Jones et al., *A direct empirical proof of the existence of dark matter*, *Astrophys. J. Lett.* **648** (2006) L109 [[astro-ph/0608407](#)].
- [4] WMAP collaboration, *Nine-Year Wilkinson Microwave Anisotropy Probe (WMAP) Observations: Cosmological Parameter Results*, *Astrophys. J. Suppl.* **208** (2013) 19 [[1212.5226](#)].
- [5] PLANCK collaboration, *Planck 2018 results. VI. Cosmological parameters*, *Astron. Astrophys.* **641** (2020) A6 [[1807.06209](#)].
- [6] M. Srednicki, R. Watkins and K. A. Olive, *Calculations of Relic Densities in the Early Universe*, *Nucl. Phys. B* **310** (1988) 693.
- [7] P. Gondolo and G. Gelmini, *Cosmic abundances of stable particles: Improved analysis*, *Nucl. Phys. B* **360** (1991) 145.
- [8] G. Jungman, M. Kamionkowski and K. Griest, *Supersymmetric dark matter*, *Phys. Rept.* **267** (1996) 195 [[hep-ph/9506380](#)].
- [9] J. L. Feng, H. Tu and H.-B. Yu, *Thermal Relics in Hidden Sectors*, *JCAP* **10** (2008) 043 [[0808.2318](#)].
- [10] J. L. Feng, *Dark Matter Candidates from Particle Physics and Methods of Detection*, *Ann. Rev. Astron. Astrophys.* **48** (2010) 495 [[1003.0904](#)].
- [11] LUX collaboration, *Improved Limits on Scattering of Weakly Interacting Massive Particles from Reanalysis of 2013 LUX Data*, *Phys. Rev. Lett.* **116** (2016) 161301 [[1512.03506](#)].
- [12] SUPERCDMS collaboration, *New Results from the Search for Low-Mass Weakly Interacting Massive Particles with the CDMS Low Ionization Threshold Experiment*, *Phys. Rev. Lett.* **116** (2016) 071301 [[1509.02448](#)].
- [13] PANDAX-II collaboration, *Dark Matter Results from First 98.7 Days of Data from the PandaX-II Experiment*, *Phys. Rev. Lett.* **117** (2016) 121303 [[1607.07400](#)].
- [14] L. Roszkowski, E. M. Sessolo and S. Trojanowski, *WIMP dark matter candidates and searches—current status and future prospects*, *Rept. Prog. Phys.* **81** (2018) 066201 [[1707.06277](#)].
- [15] T. Lin, *Dark matter models and direct detection*, *PoS* **333** (2019) 009 [[1904.07915](#)].
- [16] A. Berlin, *WIMPs with GUTs: Dark Matter Coannihilation with a Lighter Species*, *Phys. Rev. Lett.* **119** (2017) 121801 [[1704.08256](#)].
- [17] E. D. Kramer, E. Kuflik, N. Levi, N. J. Outmezguine and J. T. Ruderman, *Heavy Thermal Dark Matter from a New Collision Mechanism*, *Phys. Rev. Lett.* **126** (2021) 081802 [[2003.04900](#)].

- [18] M. Garny, J. Heisig, B. Lülfi and S. Vogl, *Coannihilation without chemical equilibrium*, *Phys. Rev. D* **96** (2017) 103521 [[1705.09292](#)].
- [19] R. T. D’Agnolo, D. Pappadopulo, J. T. Ruderman and P.-J. Wang, *Thermal Relic Targets with Exponentially Small Couplings*, *Phys. Rev. Lett.* **124** (2020) 151801 [[1906.09269](#)].
- [20] H. Kim and E. Kuflik, *Superheavy Thermal Dark Matter*, *Phys. Rev. Lett.* **123** (2019) 191801 [[1906.00981](#)].
- [21] L. J. Hall, K. Jedamzik, J. March-Russell and S. M. West, *Freeze-In Production of FIMP Dark Matter*, *JHEP* **03** (2010) 080 [[0911.1120](#)].
- [22] N. Bernal, M. Heikinheimo, T. Tenkanen, K. Tuominen and V. Vaskonen, *The Dawn of FIMP Dark Matter: A Review of Models and Constraints*, *Int. J. Mod. Phys. A* **32** (2017) 1730023 [[1706.07442](#)].
- [23] G. Bélanger, S. Chakraborti and A. Pukhov, *Feebly-interacting dark matter*, [2309.00491](#).
- [24] D. Pappadopulo, J. T. Ruderman and G. Trevisan, *Dark matter freeze-out in a nonrelativistic sector*, *Phys. Rev. D* **94** (2016) 035005 [[1602.04219](#)].
- [25] C. Cheung, G. Elor, L. J. Hall and P. Kumar, *Origins of Hidden Sector Dark Matter I: Cosmology*, *JHEP* **03** (2011) 042 [[1010.0022](#)].
- [26] X. Chu, T. Hambye and M. H. G. Tytgat, *The Four Basic Ways of Creating Dark Matter Through a Portal*, *JCAP* **05** (2012) 034 [[1112.0493](#)].
- [27] T. Hambye, M. H. Tytgat, J. Vandecasteele and L. Vanderheyden, *Dark matter from dark photons: A taxonomy of dark matter production*, *Physical Review D* **100** (2019) .
- [28] J. A. Evans, C. Gaidau and J. Shelton, *Leak-in Dark Matter*, *JHEP* **01** (2020) 032 [[1909.04671](#)].
- [29] Y. Du, F. Huang, H.-L. Li and J.-H. Yu, *Freeze-in Dark Matter from Secret Neutrino Interactions*, *JHEP* **12** (2020) 207 [[2005.01717](#)].
- [30] G. Krnjaic, *Freezing In, Heating Up, and Freezing Out: Predictive Nonthermal Dark Matter and Low-Mass Direct Detection*, *JHEP* **10** (2018) 136 [[1711.11038](#)].
- [31] J. Berger, D. Croon, S. El Hedri, K. Jedamzik, A. Perko and D. G. E. Walker, *Dark matter amnesia in out-of-equilibrium scenarios*, *JCAP* **02** (2019) 051 [[1812.08795](#)].
- [32] A. Ghosh, S. Gope and S. Mukhopadhyay, *Cannibal dark matter decoupled from the standard model: Cosmological constraints*, *Phys. Rev. D* **106** (2022) 103515 [[2206.11046](#)].
- [33] S. Ganguly, S. Roy and A. Tapadar, *Secluded dark sector and muon ( $g-2$ ) in the light of fast expanding Universe*, *JCAP* **02** (2023) 044 [[2208.13608](#)].
- [34] M. A. Buen-Abad, R. Emami and M. Schmaltz, *Cannibal Dark Matter and Large Scale Structure*, *Phys. Rev. D* **98** (2018) 083517 [[1803.08062](#)].
- [35] M. Pospelov, A. Ritz and M. B. Voloshin, *Secluded WIMP Dark Matter*, *Phys. Lett. B* **662** (2008) 53 [[0711.4866](#)].
- [36] A. Tapadar, S. Ganguly and S. Roy, *Non-adiabatic evolution of dark sector in the presence of  $U(1)_{L\mu - L\tau}$  gauge symmetry*, *JCAP* **05** (2022) 019 [[2109.13609](#)].
- [37] D. Hooper and L. Goodenough, *Dark Matter Annihilation in The Galactic Center As Seen by the Fermi Gamma Ray Space Telescope*, *Phys. Lett. B* **697** (2011) 412 [[1010.2752](#)].
- [38] FERMI-LAT collaboration, *Fermi-LAT Observations of the Diffuse Gamma-Ray Emission: Implications for Cosmic Rays and the Interstellar Medium*, *Astrophys. J.* **750** (2012) 3 [[1202.4039](#)].

- [39] FERMI-LAT collaboration, *Fermi-LAT Observations of High-Energy  $\gamma$ -Ray Emission Toward the Galactic Center*, *Astrophys. J.* **819** (2016) 44 [[1511.02938](#)].
- [40] S. Su and B. Thomas, *The LHC Discovery Potential of a Leptophilic Higgs*, *Phys. Rev. D* **79** (2009) 095014 [[0903.0667](#)].
- [41] J. Cao, P. Wan, L. Wu and J. M. Yang, *Lepton-specific two-higgs-doublet model: Experimental constraints and implication on higgs phenomenology*, *Phys. Rev. D* **80** (2009) 071701.
- [42] H. E. Logan and D. MacLennan, *Charged Higgs phenomenology in the lepton-specific two Higgs doublet model*, *Phys. Rev. D* **79** (2009) 115022 [[0903.2246](#)].
- [43] D. Phalen, B. Thomas and J. D. Wells, *Model-independent description and large hadron collider implications of suppressed two-photon decay of a light Higgs boson*, *Phys. Rev. D* **75** (2007) 117702 [[hep-ph/0612219](#)].
- [44] F. D’Eramo, N. Fernandez and S. Profumo, *When the Universe Expands Too Fast: Relentless Dark Matter*, *JCAP* **05** (2017) 012 [[1703.04793](#)].
- [45] F. D’Eramo, N. Fernandez and S. Profumo, *Dark Matter Freeze-in Production in Fast-Expanding Universes*, *JCAP* **02** (2018) 046 [[1712.07453](#)].
- [46] N. Bernal, F. Elahi, C. Maldonado and J. Unwin, *Ultraviolet Freeze-in and Non-Standard Cosmologies*, *JCAP* **11** (2019) 026 [[1909.07992](#)].
- [47] Z.-F. Chang, Z.-X. Chen, J.-S. Xu and Z.-L. Han, *FIMP Dark Matter from Leptogenesis in Fast Expanding Universe*, *JCAP* **06** (2021) 006 [[2104.02364](#)].
- [48] B. Spokoiny, *Deflationary universe scenario*, *Phys. Lett. B* **315** (1993) 40 [[gr-qc/9306008](#)].
- [49] Y. Gouttenoire, G. Servant and P. Simakachorn, *Kination cosmology from scalar fields and gravitational-wave signatures*, [2111.01150](#).
- [50] S. Heeba, F. Kahlhoefer and P. Stöcker, *Freeze-in production of decaying dark matter in five steps*, *JCAP* **11** (2018) 048 [[1809.04849](#)].
- [51] A. Hryczuk and M. Laletin, *Dark matter freeze-in from semi-production*, *JHEP* **06** (2021) 026 [[2104.05684](#)].
- [52] P. Bandyopadhyay, E. J. Chun and J.-C. Park, *Right-handed sneutrino dark matter in  $U(1)'$  seesaw models and its signatures at the LHC*, *JHEP* **06** (2011) 129 [[1105.1652](#)].
- [53] M. Farina, D. Pappadopulo, J. T. Ruderman and G. Trevisan, *Phases of Cannibal Dark Matter*, *JHEP* **12** (2016) 039 [[1607.03108](#)].
- [54] D. Tytler, J. M. O’Meara, N. Suzuki and D. Lubin, *Review of Big Bang nucleosynthesis and primordial abundances*, *Phys. Scripta T* **85** (2000) 12 [[astro-ph/0001318](#)].
- [55] M. Kawasaki, K. Kohri, T. Moroi, K. Murai and H. Murayama, *Big-bang nucleosynthesis with sub-GeV massive decaying particles*, *JCAP* **12** (2020) 048 [[2006.14803](#)].
- [56] K. Jedamzik, *Big bang nucleosynthesis constraints on hadronically and electromagnetically decaying relic neutral particles*, *Phys. Rev. D* **74** (2006) 103509 [[hep-ph/0604251](#)].
- [57] M. Kawasaki, K. Kohri, T. Moroi and Y. Takaesu, *Revisiting Big-Bang Nucleosynthesis Constraints on Long-Lived Decaying Particles*, *Phys. Rev. D* **97** (2018) 023502 [[1709.01211](#)].
- [58] J. R. Alves, L. Angel, L. Guedes, R. M. P. Neves, F. S. Queiroz, D. R. da Silva et al., *Updated Big Bang Nucleosynthesis Bounds on Long-lived Particles from Dark Sectors*, [2311.07688](#).
- [59] T. Kanzaki, M. Kawasaki, K. Kohri and T. Moroi, *Cosmological Constraints on Neutrino Injection*, *Phys. Rev. D* **76** (2007) 105017 [[0705.1200](#)].

- [60] A. W. Strong, I. V. Moskalenko and O. Reimer, *Evaluation of models for diffuse continuum gamma-rays in EGRET range*, in *28th International Cosmic Ray Conference*, pp. 2309–2312, 6, 2003, [astro-ph/0306346](#).
- [61] A. W. Strong, I. V. Moskalenko and O. Reimer, *Diffuse galactic continuum gamma rays. A Model compatible with EGRET data and cosmic-ray measurements*, *Astrophys. J.* **613** (2004) 962 [[astro-ph/0406254](#)].
- [62] T. Bringmann and C. Weniger, *Gamma Ray Signals from Dark Matter: Concepts, Status and Prospects*, *Phys. Dark Univ.* **1** (2012) 194 [[1208.5481](#)].
- [63] R. Essig, E. Kuflik, S. D. McDermott, T. Volansky and K. M. Zurek, *Constraining Light Dark Matter with Diffuse X-Ray and Gamma-Ray Observations*, *JHEP* **11** (2013) 193 [[1309.4091](#)].
- [64] T. R. Slatyer, *Indirect Detection of Dark Matter*, in *Theoretical Advanced Study Institute in Elementary Particle Physics: Anticipating the Next Discoveries in Particle Physics*, pp. 297–353, 2018, DOI [[1710.05137](#)].
- [65] J. F. Navarro, C. S. Frenk and S. D. M. White, *The Structure of cold dark matter halos*, *Astrophys. J.* **462** (1996) 563 [[astro-ph/9508025](#)].
- [66] J. F. Navarro, C. S. Frenk and S. D. M. White, *A Universal density profile from hierarchical clustering*, *Astrophys. J.* **490** (1997) 493 [[astro-ph/9611107](#)].
- [67] M. Cirelli, G. Corcella, A. Hektor, G. Hutsi, M. Kadastik, P. Panci et al., *PPPC 4 DM ID: A Poor Particle Physicist Cookbook for Dark Matter Indirect Detection*, *JCAP* **03** (2011) 051 [[1012.4515](#)].